npj Regenerative Medicine

https://doi.org/10.1038/s41536-026-00492-9

Article in Press

TGF-alpha/EGFR signalling mediates retinoic acid-induced lung repair

Received: 24 September 2025

Accepted: 23 June 2026

Published online: 04 July 2026

Cite this article as: Cheong, S.-S., Yan, C., Mongey, R. *et al.* TGF-alpha/EGFR signalling mediates retinoic acid-induced lung repair. *npj Regen Med* (2026). https://doi.org/10.1038/s41536-026-00492-9

Sek-Shir Cheong, Chunyu Yan, Róisín Mongey, David Chambers, Mark Griffiths, Matthew Hind & Charlotte H. Dean

We are providing an unedited version of this manuscript to give early access to its findings. Before final publication, the manuscript will undergo further editing. Please note there may be errors present which affect the content, and all legal disclaimers apply.

If this paper is publishing under a Transparent Peer Review model then Peer Review reports will publish with the final article.

ARTICLE IN PRESS

© The Author(s) 2026. **Open Access** This article is licensed under a Creative Commons Attribution 4.0 International License, which permits use, sharing, adaptation, distribution and reproduction in any medium or format, as long as you give appropriate credit to the original author(s) and the source, provide a link to the Creative Commons licence, and indicate if changes were made. The images or other third party material in this article are included in the article's Creative Commons licence, unless indicated otherwise in a credit line to the material. If material is not included in the article's Creative Commons licence and your intended use is not permitted by statutory regulation or exceeds the permitted use, you will need to obtain permission directly from the copyright holder. To view a copy of this licence, visit http://creativecommons.org/licenses/by/4.0/.

ARTICLE IN PRESS

TGF-alpha/EGFR signalling mediates retinoic acid-induced lung repair

Sek-Shir Cheong[1], Chunyu Yan[1], Róisín Mongey[1], David Chambers[2], Mark Griffiths[1,3], Matthew Hind[1,4], Charlotte H. Dean[1]*

[1]National Heart and Lung Institute (NHLI), Imperial College London, London, UK

[2]Wolfson Centre for Age Related Diseases, King's College London, London, UK

[3]Peri-Operative Medicine Department, St Bartholomew's Hospital, London, UK

[4]National Institute for Health Research (NIHR) Respiratory Biomedical Research Unit at the Royal Brompton & Harefield NHS Foundation Trust, London, UK

Correspondence: Charlotte H. Dean

Email: c.dean@imperial.ac.uk; Tel: +442075943174

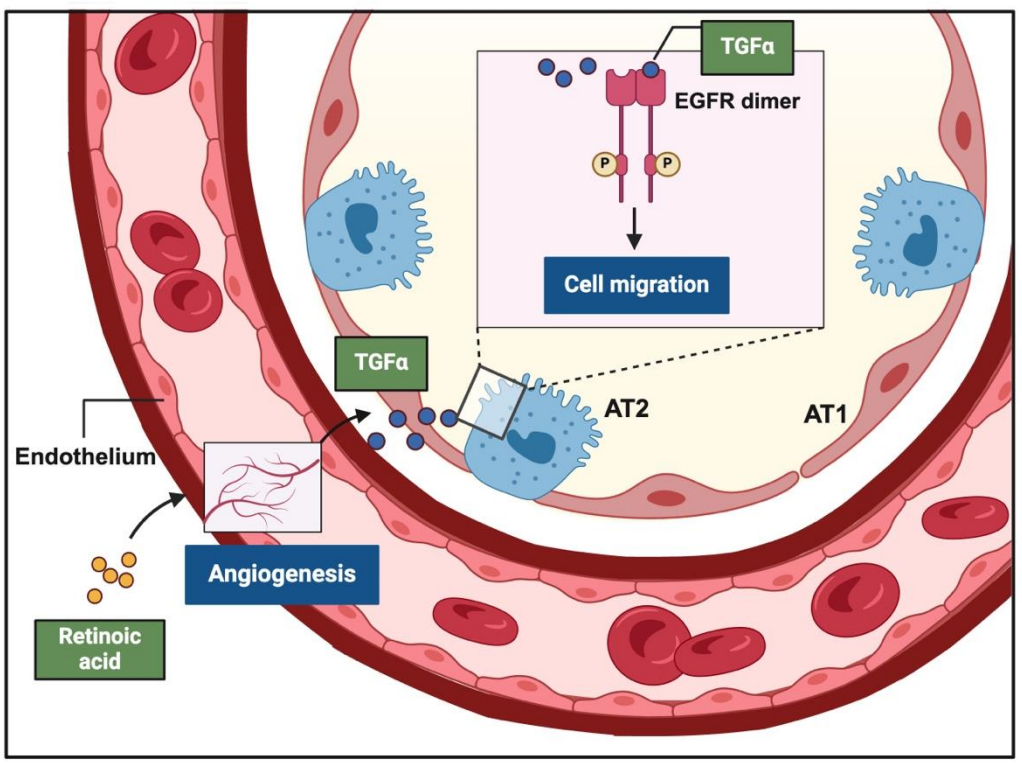
Keywords: TGF-alpha, retinoic acid, EGFR signalling, angiogenesis, alveolar repair, pulmonary microvascular endothelial cells, lung repair, cell migration

ARTICLE IN PRESS

Abstract

Lung repair involves coordination of multicellular processes, including endothelial angiogenesis and epithelial repopulation. Retinoic acid (RA) signalling is crucial for lung development, homeostasis, and repair, however, the mechanisms through which RA drives repair are still unknown. It has previously been shown that RA has no direct effects on repair of alveolar epithelium, yet in animal studies, RA induces alveolar regeneration. Here we show that RA induces endothelial angiogenesis, which is associated with enhanced paracrine signalling to alveolar epithelial cells. Transcriptomic profiling of RA-treated HPMECs undergoing angiogenesis revealed enrichment of wound healing pathways and subsequent in-silico analysis identified

several candidate mediators of endothelial-epithelium crosstalk. Scratch assays demonstrated that of these candidates, only TGFα promoted wound healing in alveolar epithelial A549 and primary human alveolar type 2 (hAT2) cells. Mechanistically, TGFα was associated with increased epithelial cell migration and activation of EGFR signalling, without detectable effects on proliferation or apoptosis. Our findings indicate that RA-induced endothelial angiogenesis promotes epithelial EGFR signalling through paracrine mediators, including TGFα. This study highlights the importance of endothelial–epithelial interactions in lung repair and provides insight into pathways that may be targeted to enhance alveolar regeneration.



ARTICLE IN PRESS

Introduction

A common denominator in many lung diseases is insufficient functional alveolar surface area for gas-exchange. The root cause of this may differ, for example in emphysema, a pathology associated with chronic obstructive pulmonary disease (COPD), the alveoli are destroyed due to repeated insults to the lungs causing tissue destruction. In the case of bronchopulmonary dysplasia, a disease of prematurity, infants fail to form an appropriate number of alveoli, leading to compromised gas-exchange requiring oxygen support and life-long increased susceptibility to other lung diseases. Currently there are no treatments capable of restoring damaged lung parenchyma but one promising avenue through which this might be achieved, is to develop a regenerative medicine treatment to repair or (re)grow alveoli [1,2].

The lungs possess significant ability to regenerate and repair following injury, and we are beginning to understand the underlying cellular mechanisms governing these processes [3]. For example, there are populations of tissue stem or progenitor cells that reside at different anatomical locations in the lungs which can become activated upon lung injury and contribute to regenerating the tissue [4,5]. In addition, other cell behaviours such as cell migration, proliferation, and cell plasticity contribute to repair of lung tissue [6]. Pharmacological-based modification of alveolar repair has begun to show real therapeutic potential for treating parenchymal lung diseases [7].

One possible approach to develop a regenerative medicine treatment is to identify the molecular signals that drive endogenous lung repair/regeneration and harness these to repair damaged lung tissue. However, this requires detailed knowledge about the endogenous pro-repair pathways. Emerging lung pro-repair factors include Wingless-type MMTV integration site family (Wnts), fibroblast growth factors (FGFs), and sonic hedgehog growth factors [8-10]. In addition, the Vitamin

ARTICLE IN PRESS

A metabolite, retinoic acid (RA) plays a critical role in lung development and alveolar regeneration [11,12].

To date, research on alveolar repair and regeneration has largely focused on the epithelial population, with comparatively less attention given to the capillary endothelium, despite its equally critical role in gas exchange [13]. RA is a well-known pro-regenerative factor across species, and studies in animal models demonstrated its ability to drive alveolar regeneration [14]. Human studies identified an imbalance between synthesis and breakdown of RA metabolism in emphysematous lungs, and RA signalling was activated in the microvascular endothelium, which stimulates angiogenesis but does not directly induce epithelial repair [15]. In addition, Ding and colleagues showed that endothelial-derived angiocrine signals induce and sustain alveolar regeneration [16]. Building on these research findings, we hypothesised that factors produced by the microvascular endothelium during RA-induced angiogenesis may act as endogenous mediators that influence alveolar epithelial repair through paracrine signalling. To test this hypothesis, we conducted microarray analysis of RA-treated lung microvascular endothelial cells undergoing angiogenesis and identified several candidate genes encoding intercellular signalling proteins. We subsequently tested the pro-repair capabilities of these proteins in vitro and found that transforming growth factor-α (TGFα) promoted repair responses in human alveolar epithelial cells, in association with activation of epidermal growth factor receptor (EGFR) signalling. TGFα, one of seven known EGFR ligands, has previously been shown to be important for alveologenesis [17]. These key mechanistic findings provide insight into potential mechanisms through which RA-regulated endothelial activity may influence epithelial repair and highlight pathways that could be explored for regenerative therapeutic strategies in chronic lung disease.

ARTICLE IN PRESS

ARTICLE IN PRESS

ARTICLE IN PRESS

Results

Increased RA signalling activity following acid injury in mouse Precision-Cut Lung Slices (PCLS)

To explore the role of RA signalling pathway in lung repair, we generated mouse PCLS and conducted quantitative real-time PCR (qRT-PCR) to assess the expression of RA pathway components in uninjured controls versus acid-injured PCLS. Acid injury was induced by exposure to 0.1 M HCl for 1 min, and mRNA levels of RA receptors (*Rara, Rarb*, and *Rarg*), RA synthesis genes (*Aldh1a1, Aldh1a2*, and *Aldh1a3*), and RA degradation genes (*Cyp26a1*, *Cyp26b1*, and *Cyp26c1*) were quantified 48 hr post-injury. As shown in Figure 1, *Rarb* and *Rarg* transcript levels were significantly increased by 4.9-fold ($p = 0.029$) and 2.3-fold ($p = 0.029$), respectively, following acid injury of mouse PCLS. The RA synthesis gene *Aldh1a3* was also significantly upregulated, showing a 2.2-fold increase ($p = 0.029$), whereas *Aldh1a2* expression decreased to 0.6-fold ($p = 0.029$). Additionally, the RA degradation genes *Cyp26a1* and *Cyp26c1* showed significant upregulation with increases of 2.5-fold ($p = 0.029$) and 1.6-fold ($p = 0.029$), respectively, compared to uninjured control PCLS. No significant changes were observed for *Rara*, *Aldh1a1*, or *Cyp26b1*.

Collectively, these data suggest an increased RA signalling activity following acid injury, highlighting a role for RA signalling in the early stages of lung repair.

RA stimulates angiogenesis and wound healing in endothelial cells, but not in alveolar epithelial cells

Our previous work demonstrated that RA induced angiogenesis in human pulmonary microvascular endothelial cells (HPMECs) [15]. As a prelude to microarray experiments, we

ARTICLE IN PRESS

replicated the experiment. Consistent with previous findings, we found that tube length, averaging 40,546 μm per field of view with RA treatment, compared to 32,225 μm in the 0.1% vehicle ethanol (EtOH) control (p = 0.0317) (Figures 2a-c). Furthermore, the total number of nodes per field of view increased from 141 in the control to 217 in RA-treated HPMECs (p = 0.0317) (Figure 2d).

To assess whether RA also modulates wound healing capacity in other endothelial cell types, scratch wound assays were performed on human umbilical vein endothelial cells (HUVECs) treated with varying concentrations of RA. Compared to vehicle EtOH-treated controls, RA significantly enhanced wound healing in a dose-dependent manner. The most pronounced effect was observed at 10 μM RA, resulting in an 80.1% wound healing compared to 38.8% in the control (p = 0.0002). Treatment with 5 μM RA led to 67.2% wound closure (p = 0.0341), while 3 μM RA increased closure to 61.0%, though this was not statistically significant. HUVECs cultured in complete endothelial growth media (EGM) with 3% foetal calf serum (FCS), serving as a positive control, exhibited high wound healing capacity (86.1%) (Figures 2e and f). However, higher RA concentrations (20 μM and 50 μM) were toxic, leading to cell death after 19 hours of incubation (Figure 2g).

We also confirmed that consistent with previous findings [15], direct treatment of the alveolar epithelial cell line A549 with RA did not induce wound healing (Figure 2h). A549 cells cultured in DMEM supplemented with 10% foetal bovine serum (FBS) served as a positive control, demonstrating nearly complete wound closure after 19 hours (Figure 2h).

Transcriptomic profiling of RA-induced responses in HPMECs

To investigate the mechanisms underlying RA-induced angiogenesis in HPMECs, transcriptomic profiling was performed to examine gene expression changes during this process. Time-lapse imaging of angiogenesis was first conducted to determine critical time points for further analysis.

ARTICLE IN PRESS

As shown in Supplementary Video S1, RA-treated HPMECs rapidly migrated and reorganised into tube-like structures within 40 minutes of seeding on Matrigel, whereas vehicle-treated (EtOH) controls remained randomly distributed at the same time point (Video S2). By 60 minutes, clear differences in tube formation were evident between control and RA-treated cells (Videos S1 and S2). By 200 minutes, extensive tube networks had formed in RA-treated HPMECs. Based on these observations, RNA was extracted at 40 min, when tube initiation was first apparent, and at 4 hr, when significant networks were evident, for whole-genome expression analysis comparing EtOH control versus RA-treated HPMECs (Figure 3a).

Microarray analysis identified 962 differentially expressed genes (DEGs) at 40 minutes and 545 DEGs at 4 hours post-treatment between control and RA-treated HPMECs [fold change > 1.5 or < -1.5, false detection rate (FDR)-adjusted p-value < 0.05] (Supplementary Tables S1 and S2). Notably, volcano plot analysis highlighted key components of the RA signalling pathway, including *RARB* (retinoic acid receptor beta), *DHRS3* (dehydrogenase/reductase 3), *NRIP1* (nuclear receptor interacting protein 1), and *RDH10* (retinol dehydrogenase 10), among the most upregulated genes at 4 hours post-RA treatment (Figures 3b and c). In contrast, none of the top genes upregulated at 40 minutes were related to RA signalling (Figure S1).

RA is the primary ligand for RAR-RXR heterodimers, which bind to retinoic acid response elements (RAREs) to initiate transcription of RA target genes [18]. To further investigate the response of HPMECs to RA, the top 15 DEGs at both the 40-minute and 4-hour time points were analysed to determine whether these genes contained a RARE motif (Supplementary Tables S3 and S4). *In silico* prediction of RARE DR5 sequences was performed using oPOSSUM3, and results were cross-referenced with previously published RARE-containing genes [19,20]. Interestingly, the top 15 upregulated genes at 4 hours showed significant enrichment for RARE-containing genes (47%; 7 out of 15 genes), including *DHRS3, RARB, NRIP1, HIC1, HOXA3,*

ARTICLE IN PRESS

HOXA5, and ARHGAP18 (Table S3). In contrast, none of the top 15 upregulated genes at 40 minutes contained RARE sequences (Table S4). These findings strongly suggest that a cellular response to exogenous RA has occurred by 4 hours post-treatment, leading us to focus our subsequent gene enrichment and functional analyses on the 4-hour dataset.

Previous studies have shown that RA induces the upregulation of vascular endothelial growth factor A (*VEGFA*) [15]. Consistent with this, our findings showed increased *VEGFA* expression at 40 minutes and upregulation of vascular endothelial growth factor receptor 1 (*VEGFR1* or *FLT1*) at 4 hours post-RA treatment. No changes were found in other genes involved in VEGF signalling, including *VEGFB*, *VEGFC, FLT4 (VEGFR3), KDR (VEGFR2),* neuropilin-1 (*NRP1*), and neuropilin-2 (*NRP2*) (Figure S2).

Enriched GO terms and pathways in RA-treated HPMECs

Since cellular responses to RA have occurred by 4 hours post-treatment (Figures 3b and c, and Table S3), we performed gene set enrichment analysis (GSEA) on DEGs from this time point using Panther and Cytoscape. Several key biological processes were significantly enriched in RA-treated HPMECs. The most prominent processes included regulation of cell adhesion, developmental processes, and actin filament organisation, all highly significant after FDR adjustment. Additional enriched processes, including epithelial cell proliferation, differentiation, cell motility, response to wounding, and tube morphogenesis, pointed to a robust cellular response to RA (Figure 4a).

Pathway enrichment analysis further confirmed activation of RA signalling in RA-treated HPMECs. Pathways directly related to RA, including retinoic acid signalling and RA biosynthesis, were significantly enriched at 4 hours post-treatment (Figure 4b). Additionally, pathways such as

ARTICLE IN PRESS

interferon signalling and CCKR signalling suggest that RA also modulates immune responses. Notably, the EGF receptor (EGFR) signalling pathway, which has been implicated in lung development [21] and various chronic pulmonary diseases, including lung fibrosis, COPD, asthma, and lung cancer [22-24], as well as lung repair [25], was also significantly enriched.

Identification of candidate paracrine mediators upregulated in RA-treated HPMECs

Lung repair requires coordinated crosstalk among alveolar cell types [26]. Since RA promoted angiogenesis and wound healing in endothelial cells but had no direct effect on alveolar epithelial cells (Figure 2), we hypothesised that RA signalling may induce the expression of pro-repair paracrine factors in endothelial cells that act on other alveolar cell populations. To identify candidate paracrine mediators, the 545 DEGs detected at 4 hours post RA-treatment were subjected to Panther "Protein classification" analysis. This revealed 14 candidate genes encoding intercellular signalling proteins, of which eight were upregulated, including *CXCL8* (C-X-C motif chemokine ligand 8), *TGFA* (transforming growth factor alpha), *BMP2* (bone morphogenetic protein 2), *FGF20* (fibroblast growth factor 20), *WNT9A* (Wnt family member 9a), *GDF15* (growth differentiation factor 15), *EFNB1* (Ephrin B1), and *ADM* (adrenomedullin) (Table 1). Three genes, *CXCL8, TGFA,* and *BMP2,* were selected for further analysis due to their known association with lung diseases and relevant biological functions [27-29]. Notably, TGFα, encoded by *TGFA,* is a ligand for the EGFR signalling pathway, which was one of the top enriched pathways in RA-treated HPMECs (Figure 4b).

To determine whether RA-induced gene expression is dependent on endothelial state, we compared transcriptional responses in RA-treated HPMECs cultured as monolayers versus undergoing angiogenesis. qRT-PCR analysis revealed that *BMP2* and *CXCL8* were consistently upregulated in response to RA under both conditions ($p < 0.05$), indicating that these genes are directly induced by RA signalling (Figure 4c and d). In contrast, *TGFA* expression was not

ARTICLE IN PRESS

significantly altered in RA-treated HPMEC monolayers (0.83-fold relative to EtOH-treated HPMEC monolayer, p = 0.314), but was significantly upregulated in RA-treated HPMECs undergoing angiogenesis (1.54-fold increase, p = 0.029; Figure 4e). *HOXA3* and *HOXA5*, were also upregulated in RA-treated HPMEC monolayers, further supporting that they are direct targets of RA signalling (Figure S3).

TGFα induces wound healing and cell migration in alveolar epithelial cells

To evaluate the effects of TGFα, BMP2, and CXCL8 on wound healing and cell migration in alveolar epithelial cells, we treated A549 cells and primary human alveolar type 2 (hAT2) epithelial cells with recombinant proteins and performed scratch wound and cell migration assays, respectively. Treatment with TGFα significantly enhanced wound healing in A549 cells in a dose-dependent manner, with the maximal effect observed at 40 ng/ml ($p < 0.0001$) compared to the untreated control (DMEM supplemented with 0.5% FBS). Treatment with 4 ng/ml TGFα also significantly increased wound closure ($p = 0.0149$) (Figures 5a and b). Additionally, immunostaining with the proliferation marker Ki67, followed by quantification of Ki67-positive cells, revealed no significant differences in cell proliferation across the various concentrations of TGFα (Figure 5c). MTT assays further confirmed that TGFα did not affect cell viability at any concentrations tested. Cells treated with 70% methanol were used as a positive control for dead cells, which exhibited significant cell death compared to the untreated control ($p = 0.0003$) (Figure S4).

Next, we replicated the scratch assay in human primary alveolar type 2 (hAT2) cells isolated from resected lung tissue, following a previously described method [30]. hAT2 cells exhibited low wound closure (10.5% to 20.8%) (Figure S5), likely due to the removal of collagen-I matrix in the scratch area, which impaired hAT2 migratory capacity. We then employed a cell migration assay to further assess the effect of TGFα on hAT2 cells. Based on the dosage-response observed in the scratch

ARTICLE IN PRESS

assay (Figure S5), we narrowed the range of TGFα concentrations for subsequent experiments to 0.2 ng/ml to 4 ng/ml. Consistent with findings in A549 cells, TGFα treatment enhanced hAT2 migration in a concentration-dependent manner, with the most pronounced effect observed at 4 ng/ml TGFα (42.5% cell migration rate) compared to 26.3% in the control (p = 0.0314) (Figures 5d and e). TGFα treatment also did not significantly impact cell proliferation (Figure 5f), and labelling of hAT2 cells with NucView 488-caspase-3 dye indicated that TGFα did not induce apoptosis (Figure 5g). MTT assays confirmed that cell viability was maintained in TGFα-treated cells. Cells treated with 70% methanol served as a positive control for dead cells, demonstrating a significant reduction in cell viability compared to the untreated control ($p < 0.0001$) (Figure S6).

The effects of BMP2 and CXCL8 on wound healing in A549 cells were also investigated; however, no significant differences were observed between treated and untreated cells at any concentrations tested (Figures S7a and b). MTT assays confirmed the concentrations of BMP2 and CXCL8 used in these experiments did not affect cell viability (Figures S7c and d).

TGFα does not modulate cell migration or proliferation in human lung fibroblasts and microvascular endothelial cells

To determine whether TGFα also influences cell migration in other alveolar cell populations, cell migration and scratch wound assays were performed on primary human lung fibroblasts (HLFs) and HPMECs, respectively. Our results demonstrated that TGFα did not significantly affect cell migration in HLFs (Figures 6a and b). Furthermore, immunostaining for the proliferation marker Ki67 revealed no effect of TGFα on cell proliferation. HLFs cultured in DMEM supplemented with 10% FBS exhibited a significantly higher percentage of Ki67-positive cells (42.9%) compared to control cells grown in DMEM containing reduced FBS (25.7%) (p = 0.0172) (Figure 6c). As shown in Figure 6d, no apoptotic cells were detected in either control or TGFα-treated HLFs, whereas

ARTICLE IN PRESS

cells treated with 70% methanol served as a positive control (Figure 6d). Similarly, TGFα had no effect on wound healing in HPMECs (Figures 6e and f). Cell viability assays confirmed that TGFα treatment did not influence metabolic activities in either HLFs or HPMECs (Figures S8a and b).

In summary, our findings demonstrate that the pro-migratory and wound healing effects of TGFα are specific to alveolar epithelial cells.

TGFα is associated with epithelial EGFR activation in response to endothelial angiogenesis

Given that TGFα is a known ligand of EGFR, we next investigated whether TGFα-induced epithelial wound healing is associated with activation of this pathway. To establish conditions under which EGFR activation could be reliably detected, A549 cells were treated with recombinant TGFα or epidermal growth factor (EGF; another EGFR ligand) and assessed by immunostaining for phospho-EGFR. No clear changes in phospho-EGFR staining were observed at 30 minutes (Figure 7a). However, after 2 hours of stimulation, both TGFα- and EGF-treated cells exhibited increased membrane-associated phospho-EGFR compared with serum-free controls (Figure 7b–c), indicating that EGFR activation is detectable at this time point.

We next sought to detect TGFα secretion from HPMECs. ELISA analysis of conditioned media collected from EtOH- or RA-treated HPMECs at 4 and 16 hours post-treatment failed to detect TGFα. Notably, although the TGFα standard provided with the ELISA kit produced a valid standard curve, commercially available recombinant TGFα spiked into culture media was also not detected, suggesting a technical limitation of the assay under these conditions (Table S5).

Given this limitation, we adopted an alternative approach to assess TGFα activity and distribution in an A549-HPMEC transwell co-culture system. A549 cells were co-cultured with RA- or EtOH-

ARTICLE IN PRESS

treated HPMECs on Matrigel, followed by immunostaining for phospho-EGFR and TGFα (Figure 8a). Increased membrane-associated phospho-EGFR was observed in A549 cells co-cultured with RA-treated HPMECs, accompanied by enrichment of TGFα signal that appeared to co-localise with phospho-EGFR at the cell membrane. This pattern was not observed in A549 cells co-cultured with EtOH-treated HPMECs (Figure 8b and c). Importantly, direct treatment of A549 cells with RA in the absence of HPMECs did not reproduce this distribution of phospho-EGFR or TGFα, supporting a paracrine mechanism (Figure 8d).

Discussion

Here we conducted a microarray to identify candidate signalling factors upregulated in RA-treated HPMECs undergoing angiogenesis. Among these, CXCL8, TGFα and BMP2 were selected for further investigation based on their degree of upregulation and biological relevance. TGFα specifically induced repair and migration of both A549 and human primary AT2 cells, whereas CXCL2 and BMP2 did not. In contrast, TGFα had no effect on repair or proliferation of either primary HLFs or HPMECs. Subsequently, using a co-culture approach, we found that RA-induced HPMEC angiogenesis was associated with activation of EGFR signalling and increased membrane-associated TGFα in adjacent A549 cells, supporting a paracrine interaction between endothelial and epithelial cells.

ARTICLE IN PRESS

It has long been appreciated that RA is a powerful regenerative agent across organs and species [31,32]. Interestingly, a recent study in the skin identified a pivotal role of RA in regulating stem cell fate during wound repair by modulating lineage plasticity; a transient state that bestows tissue stem cells with fate flexibility and is important in the repair response to injury [33]. In the lung, RA is critical for development and has been implicated in alveolar regeneration [11,34]. Epidemiological

ARTICLE IN PRESS

studies further demonstrate that vitamin A deficiency has detrimental effects not only on the lungs but also other organ systems [35]. Promising data from animal experiments and population studies led to clinical trials being conducted with the aim of determining whether RA might be an effective treatment for patients with emphysema. Although the results of these first human lung regenerative clinical trials were largely disappointing and failed to meet their primary end points, in one trial, involving patients with CT-confirmed smoking-related emphysema, post-hoc subgroup analysis found that patients with predominantly lower-zone disease experienced reduced declines in FEV1, gas diffusion, and exercise capacity compared with placebo [36]. These findings highlight the need for a deeper mechanistic understanding of RA-driven repair processes.

We previously showed that instead of directly promoting epithelial repair, RA induced angiogenesis in HPMECs [15]. We therefore hypothesised that RA may indirectly influence alveolar epithelial repair through paracrine signalling associated with endothelial angiogenesis. To investigate this, we combined the use of human cell-based and 3D *ex vivo* models with detailed mechanistic studies of RA-driven responses in the lung. Our findings support this hypothesis by demonstrating that RA-induced angiogenesis in HPMECs is associated with upregulation of TGFα and activation of EGFR signalling in alveolar epithelial cells. Furthermore, exogenous TGFα enhanced epithelial repair responses, suggesting a potential role for TGFα in endothelial–epithelial crosstalk.

TGFα is one of seven ligands that bind to EGFR with varying affinities [37]. Considerable evidence has demonstrated a role for EGF ligands and EGFR signalling in lung repair [38]. However, although TGFα is expressed in the lungs throughout the life course, its role in repair and regeneration remains unclear. While overexpression studies in mice have linked TGFα to pathological remodelling, including alveolar airspace enlargement and fibrosis, these effects appear to be dose-dependent [17]. TGFα is also upregulated in lung diseases characterised by tissue damage, including idiopathic pulmonary fibrosis (IPF), COPD, and in post-COVID patients (39-41).

ARTICLE IN PRESS

Although this has often been interpreted as detrimental, it could equally reflect a context-dependent adaptive repair response, with TGFα contributing positively to lung regeneration. Recently, Li and colleagues showed that lipopolysaccharide (LPS) injury induces upregulation of TGFα/EGFR signalling, leading to abnormal elastin deposition and alveolar simplification; inhibition of EGFR with erlotinib mitigated these effects on alveoli, underscoring the need for tight regulation of TGFα levels and highlighting the TGFα-EGFR axis as a potential therapeutic target to modulate alveolar regeneration [17,39].

Consistent with a context-dependent role, in our current study, *TGFA* mRNA was not increased in RA-treated HPMEC monolayers but was upregulated during RA-induced angiogenesis. This suggests that *TGFA* induction is not a direct effect of RA treatment but rather a response linked to the angiogenic state, supporting our hypothesis that endothelial activation during angiogenesis promotes paracrine signalling that mediates epithelial repair. This contrasts with a previous study reporting suppression of *TGFA* expression in upper airway epithelial cells and airway explants treated with retinol [40]. Notably, our study used retinoic acid (a derivative of retinol) at 10 μM compared with 0.1 μM retinol in Miller's work and focused on alveolar cells rather than airway epithelial cells or tissues, suggesting that *TGFA* transcriptional responses to retinoids are tightly regulated, both dose- and context-dependently.

The validity of the microarray data was confirmed by the enrichment of RA signalling pathways in HPMECs 4 hours after RA treatment. GO analysis highlighted two major aspects of RA-induced changes: first, reorganisation of actin filaments, which governs cell adhesion and migration, processes essential for wound healing and tissue repair, and second, changes in epithelial cell behaviour, supporting the idea of crosstalk between HPMECs and epithelial cells in response to exogenous RA exposure.

ARTICLE IN PRESS

However, in the current study, we were unable to detect TGFα in supernatants collected from A549-HPMEC co-cultures. While the ELISA assay produced a valid standard curve, TGFα was not detected in co-culture supernatants, or in culture media supplemented with recombinant TGFα, which was included as a positive control (Table S5). This suggests methodological limitations, potentially suboptimal timing of supernatant collection or limited recognition of specific TGFα isoform(s) by the antibodies used. Notably, multiple isoforms of TGFα are annotated in Ensembl, which could contribute to antigen-antibody mismatch. Despite this limitation, we observed membrane-associated TGFα together with activation of EGFR signalling in A549 cells exposed to RA-treated HPMECs undergoing angiogenesis in co-culture, supporting a paracrine mechanism.

Ideally, mechanistic confirmation could be obtained by blocking a TGFα-specific EGFR phosphorylation site. However, no known TGFα-specific EGFR phosphorylation sites have been identified to date[41]. Interrogating the specific contribution of an individual EGFR ligand such as TGFα is further complicated by the well-established redundancy within the EGFR ligand family. EGFR signalling is mediated by a network of ligands with overlapping and partially redundant functions in epithelial systems[42,43]. This is supported by genetic studies demonstrating that combined loss of multiple EGFR ligands does not phenocopy EGFR deficiency. Specifically, mice lacking EGF, TGFα and amphiregulin remain viable and display relatively mild developmental defects, in contrast to EGFR-null mice, which exhibit severe epithelial abnormalities and perinatal lethality. Notably, despite the absence of these three ligands, ERK activation in mammary epithelial structures was largely preserved, indicating that EGFR signalling can be maintained through compensatory activity from remaining ligands[44]. Consistent with this, experimental studies have demonstrated that disruption of individual EGFR ligands is insufficient to abrogate downstream signalling, whereas simultaneous ablation of multiple ligands is required to

ARTICLE IN PRESS

significantly impair pathway activation, highlighting the inherent functional redundancy of the EGFR ligand network[41].

In line with this, we attempted to block TGFα using a neutralising antibody in our system. However, this did not reduce EGFR activation (Figure S9), consistent with compensatory activity from other EGFR ligands. While global EGFR inhibition (e.g. using tyrosine kinase inhibitors such as erlotinib) has been shown to modulate epithelial repair, this approach would not allow us to address the specific role of TGFα. Instead, it would introduce significant confounding effects by simultaneously blocking all EGFR ligands, thereby broadly impairing epithelial repair processes, given the well-established role of EGFR signalling in epithelial cell migration, proliferation, and wound healing.

To further assess the functional relevance of endothelial-derived signals, we evaluated epithelial wound closure in response to conditioned media from RA-treated HPMECs. However, under these experimental conditions, no significant differences in wound healing rates were observed (Figure S10). Notably, our dose–response experiments demonstrated that TGFα promotes epithelial migration within a defined concentration range, suggesting that a threshold level of stimulation is required to elicit measurable effects on wound closure. In contrast, endothelial-derived TGFα in the co-culture system is likely present at lower abundance and may be spatially restricted or transient in nature. These conditions may be sufficient to activate EGFR signalling, as evidenced by increased membrane-associated phospho-EGFR, but insufficient to drive detectable changes in the functional assay. Consistent with this, membrane-bound pro-TGFα has been shown to activate EGFR on adjacent cells without requiring accumulation of soluble ligand[45], and EGFR ligands are known to signal through localised juxtacrine/paracrine mechanisms[37]. These findings highlight the distinction between pathway activation and downstream functional outcomes and suggest that additional factors or more physiologically relevant systems may be required to fully recapitulate endothelial–epithelial repair dynamics.

ARTICLE IN PRESS

In summary, this study shows that RA induces angiogenesis in lung endothelial cells, leading to activation of EGFR signalling in alveolar epithelial cells via paracrine mediators, including TGFα. More broadly, our findings highlight the importance of using physiologically relevant human models to uncover the detailed mechanisms of tissue repair required for the development of effective pharmacological regenerative medicine treatments.

Methods

Sex as a biological variable

Human tissue, for cell isolation, was obtained from both males and females.

Ethics approval

Lung tissue samples were collected from male and female patients undergoing lung resection at the Royal Brompton & Harefield hospital (RBHT), by Biobank sample co-ordinators within the RBHT Clinical Research Facility (CRF). All samples were obtained following informed consent from patients. The research was conducted using the RBHT Biobank ethics number: 20/SC/0142.

Mice

All animal maintenance and procedures were conducted in compliance with the requirements of the Animal (Scientific Procedures) Act 1986. Animal work was approved by the South Kensington AWERB committee at Imperial College London. Mice were housed in specific pathogen-free conditions and given food and water *ad libitum*. Wild-type female mice aged 10-12 weeks were purchased from Charles River (United Kingdom).

Mouse Precision-Cut Lung Slices (PCLS) and acid injury

ARTICLE IN PRESS

Mouse PCLS were generated following previously established protocols [46,47]. Briefly, adult mice were euthanised via intraperitoneal injection of pentobarbital. The anterior chest and neck wall were carefully dissected, and a small incision was made in the trachea below the cricoid cartilage. A 21G rigid metal cannula was inserted into the trachea incision, and the lungs were inflated by injecting 1.2 ml of 2% (w/v) low-gelling agarose (Sigma–Aldrich, A9414) dissolved in 1× Hank's Balanced Salt Solution (HBSS; Life Technology, 14025100) containing 1% HEPES buffer (Life Technology, 15630080). The chest cavity was cooled with ice to solidify the agarose.

The lungs and heart were excised and submerged in ice-cold HBSS/HEPES buffer. Lung lobes were carefully separated and sliced transversely at a thickness of 300 µm using an automated vibratome (Compresstome VF-300-0Z; Precisionary Instruments LLC) in ice-cold HBSS/HEPES buffer. PCLS were then transferred to 24-well plates containing ice-cold serum-free (SF) Dulbecco's Modified Eagle Medium (DMEM)-GlutaMAX (Life Technologies, 31966021) with 1% penicillin-streptomycin (Merck, P0781). PCLS were incubated overnight at 37°C in a 5% CO_2 atmosphere and washed three times with warm SF-DMEM to remove any remaining agarose.

ARTICLE IN PRESS

For acid injury, PCLS were treated with 0.1 M HCl (Fisher Chemical, 10053023) for 1 minute at room temperature (RT). The HCl solution was then discarded, and PCLS were washed three times with phosphate-buffered saline (PBS; Sigma; D8537) to remove residual acid. PCLS were cultured in fresh SF-DMEM for 48 hours before RNA extraction.

Cell culture

Primary human pulmonary microvascular endothelial cells (HPMECs; Promocell, C12281) and human umbilical vein endothelial cells (HUVECs; Promocell, C12200) were cultured in Endothelial Cell Growth Medium MV (EGM-MV; Promocell, C22020) and Endothelial Growth Media (EGM; Promocell, C-22010), respectively. Cells were maintained at 37°C in a 5% CO_2 atmosphere. Cells

ARTICLE IN PRESS

were used between passages 3 and 7, showing no changes in morphology or baseline tube-forming capacity. HPMECs used in this study were sourced from two Caucasian female donors, aged 64 and 98. A549 cells, a human alveolar adenocarcinoma epithelial cell line, were purchased from the American Type Culture Collection (ATCC). Cells were cultured in DMEM-GlutaMAX (Gibco) supplemented with 10% foetal bovine serum (FBS; Sigma, F9665) and 1% penicillin/streptomycin at 37°C with 5% CO_2.

The research carried out in this manuscript adheres to the World Medical Association declaration of Helsinki.

Primary human alveolar type 2 (hAT2) epithelial cells and human lung fibroblasts (HLFs) were isolated from histologically normal lung tissues obtained from patients undergoing surgical resection for suspected lung tumours, Lung tissue samples were collected from patients undergoing lung resection at the Royal Brompton Hospital (RBH), by Biobank sample co-ordinators within the RBH Clinical Research Facility. All samples were obtained following informed consent from patients. The research was conducted under the National Research Ethics Service (NRES) reference number: 20/SC/0142. The isolation protocol was based on a previously described method [30] with slight modifications.

Briefly, lung tissue was perfused with HBSS (Invitrogen, 14025-050) to remove blood and debris, followed by digestion with 0.25% trypsin (Sigma, T8003) at 37°C for 45 minutes. Trypsinisation was halted by adding FBS, and the tissue was finely chopped. DNase I (Sigma, DN25) was added to facilitate degradation of extracellular DNA to improve tissue dissociation. The resulting tissue suspension was passed through a tea strainer and a 40-µm mesh filter (Marathon Lab Supplies, 352340) to remove undigested tissue. The filtrate was centrifuged at 1,300 rpm for 10 minutes at 12°C. The pellet was resuspended in hybridoma serum-free medium (SFM; Gibco, 11570416) containing 50 µg/ml DNase I and incubated at 37°C for 45 minutes to remove immune cells.

ARTICLE IN PRESS

After incubation, the supernatant was collected and centrifuged again at 1,300 rpm for 10 minutes at 12°C. The pellet was resuspended in hybridoma medium containing 10% FBS and incubated at 37°C for 2 hours. Cells adhering to the dishes after this period were identified as HLFs, which were subsequently cultured in DMEM-GlutaMAX supplemented with 10% FBS for downstream experiments. The supernatant containing non-adherent cells was centrifuged at 1,300 rpm for 10 minutes at 12°C, and the resulting pellet, containing hAT2 cells, was resuspended and cultured in hybridoma medium with 10% FBS. hAT2 cells were not passaged, and all experiments involving these cells were completed within 68 hours of seeding. HLFs were used between passages 3-7 for experiments.

The specificity of isolated hAT2 cell populations was confirmed by immunostaining with alveolar cell type-specific markers. The hAT2 cells were positive for pan-cytokeratin (a pan-epithelial marker) and Pro-SPC (an AT2 cell marker), but negative for vimentin (a fibroblast marker) and podoplanin (PDPN; an AT1 cell marker) (Figure S11).

ARTICLE IN PRESS

Pharmacological treatment

Retinoic acid (RA; Sigma, R2625) used in this study was dissolved in absolute ethanol (EtOH; Sigma-Aldrich, 51976). Recombinant human TGFα (catalogue number: 239-A1-100), BMP2 (catalogue number: 355-BM-010), and CXCL8 (catalogue number: 208-IL-010) were obtained from R&D Systems and reconstituted according to the manufacturer's instructions. Human EGF was sourced from Promocell (catalogue number: C-39220).

Matrigel-based angiogenesis assay and tube quantification

ARTICLE IN PRESS

Angiogenesis µ-slides (Ibidi, 81506) or 24-well plates (Ibidi, 2401) were pre-coated with growth factor-reduced Matrigel (BD Biosciences, 354230), diluted to a concentration of 5 mg/ml with pre-chilled endothelial cell basal medium (EBM; Promocell, C-22220) without supplements. The plates were incubated at 37°C for 1 hour to allow the Matrigel to solidify. HPMECs were serum-starved for 24 hours prior to conducting the tube formation assays. Cells were seeded at a density of 4,750 cells per well for the angiogenesis µ-slides and 70,000 cells per well for the 24-well plates. Cells were treated with either the vehicle (EtOH) or 10 µM RA.

For time-lapse imaging of tube formation, the µ-slide was immediately transferred to a pre-equilibrated, humidified incubator chamber (37°C, 5% CO_2, and approximately 21% oxygen levels) of an inverted Zeiss Axio Observer widefield epifluorescence microscope. Imaging was performed over a 4-hour period using an EC Plan-Neofluar 10×/0.30 objective lens. The total tube length and the total number of nodes per field of view were quantified using FIJI software. Data were expressed as the mean total tube length or total number of nodes per field of view.

ARTICLE IN PRESS

RNA extraction and quantitative real-time PCR (qRT-PCR)

Mouse PCLS were homogenised using a FastPrep-24TM Tissue Homogeniser (MP Biomedicals), and total RNA was extracted with the RNeasy mini kit (Qiagen, 74104) following the manufacturer's protocols. For each experimental condition, RNA samples were pooled from three PCLS, and a total of three RNA samples were prepared per condition. RNA was also extracted from HPMEC monolayers using the same RNeasy mini kit. For HPMECs cultured on Matrigel, Matrigel was first dissolved using Cell Recovery Solution (Corning, 354253) according to the manufacturer's instructions, prior to RNA extraction. RNA concentration and integrity were assessed using the TapeStation 2200 system (Agilent), and only samples with an RNA integrity number (RIN) greater than 8 were used for downstream cDNA synthesis and qRT-PCR.

ARTICLE IN PRESS

Approximately 200 ng of total RNA was reverse transcribed into cDNA using the High-Capacity cDNA Reverse Transcription kit (Applied Biosystems) according to manufacturer's instructions. Quantitative RT-PCR was then performed using TaqMan Fast Advanced Master Mix (Life Technologies) on a 7500 Fast Real-Time PCR system (Applied Biosystems). The housekeeping gene *B2m* was used as a reference for normalisation. Relative gene expression levels were calculated using the 2−ΔΔCT method. Each sample was tested in triplicate, with four biological replicates derived from four different mice.

The following TaqMan primers (Life Technologies) were used in this study: mouse *B2m* (Mm00437762_m1), human *B2M* (Hs00984230_m1), *Rara* (Mm01296312_m1), *Rarb* (Mm01319677_m1), *Rarg* (Mm00441083_m1), *Aldh1a1* (Mm00657317_m1), *Aldh1a2* (Mm00501306_m1), *Aldh1a3* (Mm00474049_m1), *Cyp26a1* (Mm00514486_m1), *Cyp26b1* (Mm00558507_m1), *Cyp26c1* (Mm03412454_m1), *TGFA* (Hs00608187_m1), *CXCL8* (Hs00174103_m1), *BMP2* (Hs00154192_m1), *HOXA3* (Hs00601076_m1), and *HOXA5* (Hs00430330_m1).

ARTICLE IN PRESS

Microarrays and raw data processing

Microarray service was provided by UK Bioinformatics Ltd. (UKB, UK). Total RNA was extracted from HPMECs cultured on Matrigel using Trizol reagent (Invitrogen, UK). RNA quality was assessed using the Agilent 2100 Bioanalyzer. For each treatment and time point, four RNA samples were prepared from independent experiments, with each sample pooled from three technical replicates (see Table S6 for sample details).

cDNA was synthesised using the Ovation® Pico WTA System V2 and labelled with the Encore Biotin Module, following the manufacturer's protocols (Nugen, USA). The labelled cDNA was hybridised to Affymetrix Human U133 Plus 2.0 Gene Chips (Affymetrix) according to the

ARTICLE IN PRESS

manufacturer's instructions. The resulting microarray data were generated in an Affymetrix CEL format and processed using the Transcriptome Analysis Console (TAC) software v4.0.2 (Thermo Scientific).

Raw data normalisation and summarisation were performed using the MAS5 algorithm within the TAC software. Gene expression analysis was conducted using the human genome reference assembly hg19. Differential expression was defined by a fold change threshold of > 1.5 or < -1.5, and a false discovery rate (FDR)-adjusted *p*-value of < 0.05. Statistical significance was calculated using moderated t-statistics from the empirical Bayes (ebayes) method within an ANOVA framework, allowing for robust identification of differentially expressed genes between RA-treated and EtOH-treated control samples. FDR correction was applied using the Benjamini-Hochberg algorithm to control for multiple testing.

Gene Set Enrichment Analysis (GSEA)

GSEA was performed to identify pathways and biological processes significantly associated with upregulated genes. Pathway enrichment analysis was conducted using PANTHER version 19.0 (www.pantherdb.org/), focusing on PANTHER Pathways and Reactome Pathways. For the enrichment of Gene Ontology (GO) biological processes, Cytoscape software version 3.10.2 was utilised, in conjunction with the STRING enrichment tool. Enriched pathways and biological processes were ranked according to their statistical significance.

Scratch wound and cell migration assays

For the scratch wound assay, 45,000 HUVECs, HPMECs, or A549 cells were seeded onto 8-well Permanox chamber slides (Fisher Scientific; 16250681), pre-coated with 2 µg/ml fibronectin (Sigma, F1141) for HUVECs and HPMECs, or 50 µg/ml rat-tail collagen I (Gibco, A1048301) for A549 cells. Cells were cultured in their respective complete media - EGM for HUVECs, EGM-MV

ARTICLE IN PRESS

for HPMECs, and DMEM-GlutaMAX supplemented with 10% FBS for A549, and incubated overnight at 37°C with 5% CO_2 to reach confluence. A scratch wound was made across the centre of the confluent monolayer using a P1000 pipette tip. Wells were gently rinsed with PBS to remove dislodged cells, followed by the addition of appropriate treatments.

For RA treatments, HUVECs were exposed to 3 μM, 5 μM, 10 μM, 20 μM, or 50 μM RA, diluted in EBM. A549 cells were treated with 10 μM of RA in SF-DMEM. Since RA was reconstituted in EtOH, control media containing 0.1% EtOH in either EBM or SF-DMEM were used for HUVECs and A549 cells, respectively. Positive control media for enhanced wound healing consisted of EGM with 3% FCS for HUVECs and DMEM supplemented with 10% FBS for A549 cells.

For the cell migration assay, hAT2 and HLFs were plated using 2-well silicone culture inserts (Ibidi, 80209) adhered to 50 μg/ml rat-tail collagen I-coated 13 mm coverslips placed in 24-well plates. Freshly isolated hAT2 cells were seeded at a density of 250,000 cells per well, while HLFs were plated at 15,000 cells per well. For HLFs, the silicone inserts were removed after overnight incubation. For hAT2 cells, debris and dead cells were gently washed off with PBS 24 hours post-seeding, and fresh hybridoma SFM supplemented with 10% FBS was added, followed by a further 24-hour incubation before insert removal. TGFα treatments were administered at appropriate concentrations in DMEM with 1% FBS for HLFs or in hybridoma SFM with 1% FBS for hAT2 cells.

Cells in both assays were imaged at time points t = 0 h and the endpoint at t = 19 h or 24 h using an inverted Zeiss Axio Observer widefield epifluorescence microscope housed in a pre-equilibrated, humidified incubator chamber (37°C, 5% CO_2, ~21% oxygen). Images were captured using an EC Plan-Neofluar 10×/0.30 objective lens, and tiling was employed to image the cell-covered areas. Wound healing percentage was quantified using a FIJI macro developed by Steve Rothery (Facility for Imaging by Light Microscopy, Imperial College London) or through manual

ARTICLE IN PRESS

analysis. For manual quantification, the wound areas were outlined with the freehand tool in FIJI, and the percentage healed was calculated by subtracting the endpoint area from the area at *t* = 0 h. Three independent experiments were conducted, and each experiment was run in triplicate.

Immunofluorescence and imaging

Cells were fixed in 4% paraformaldehyde (PFA) for 10 minutes at RT, followed by PBS. Permeabilisation was carried out using 0.2% (v/v) Triton X-100 in PBS RT for 5 minutes at RT. Blocking was then performed for 1 hour at RT using PBSBT buffer, which contains 3% bovine serum albumin (BSA) and 0.1% Triton X-100 in PBS. After blocking, cells were incubated overnight at 4°C with primary antibodies diluted in PBSBT blocking buffer. The following primary antibodies were used in this study: rabbit anti-vimentin (Bioorbyt, orb304659; 1:200), mouse anti-pan-cytokeratin (Sigma–Aldrich, C2931; 1:200), rabbit anti-Pro-SP-C (Abcam, ab90716; 1:300), hamster anti-PDPN (Developmental Studies Hybridoma Bank, 8.1.1; 1:50), rat anti-Ki67 (eBioscience, 14-5698-82; 1:500), rabbit anti-phospho-EGFR Y1068 (Cell Signalling Technology, 3777S; 1:100), and goat anti-TGF-alpha (R&D Systems, AF-239-NA; 1:30).

ARTICLE IN PRESS

Following three washes with PBS, cells were incubated for 1 hour at RT with rhodamine phalloidin (Biotium, 00027; 1:300) and species-specific Alexa Fluor 488, 594, and 647 secondary antibodies (Thermo Fisher Scientific; 1:500). After further PBS washes, cell nuclei were stained with DAPI (Thermo Scientific, 62249). Coverslips were mounted with ProLong Gold Antifade Mountant (Invitrogen, P36930). Imaging was performed using a Leica SP8 inverted confocal microscope equipped with a HC PL APO 10×/0.40 air objective lens or a HC PL APO 40×/1.30 oil objective lens. For some experiments, channel colours were changed during image post-processing to improve visual clarity.

MTT assay

ARTICLE IN PRESS

To evaluate the impact of pharmacological treatments on cell viability, an MTT assay was conducted according to the manufacturer's instructions (Roche, 11465007001). Briefly, 150 µl of 10% MTT solution diluted in serum-free media was added to each well of a 96-well plate and incubated at 37°C for 45 minutes. The resulting formazan crystals, which formed in viable cells, were solubilised by adding an equal volume of DMSO and incubating at 37°C for 10 minutes. 100 µl of eluted formazan solution was measured spectrophotometrically, with absorbance recorded at 570 nm and corrected at 690 nm using a plate reader.

Caspase-3 assay

To identify apoptotic cells, the NucView® 488 Caspase-3 assay kit (Biotium; 30029-T) was employed, following the manufacturer's protocols. At the end point of pharmacological treatments, cells were incubated with 5 µM NucView 488 substrate (prepared as 1:40 stock dilution) in the dark at RT for 30 minutes. After incubation, the dye was removed, and cells were gently washed three times with PBS. Cells were then fixed with 4% PFA for 10 minutes at RT. After fixation, the PFA was discarded, and the cells were washed three times with PBS. Cells were counterstained with DAPI at RT for 5 minutes and washed once with PBS. Cells were then mounted using ProLong® Gold Antifade Reagent and imaged on the same day using a Leica SP8 inverted confocal microscope equipped with a HC PL APO 40×/1.30 oil objective lens.

Transwell insert-based co-culturing of HPMECs and A549

HPMECs and A549 cells were co-cultured as illustrated in Figure 8a. A549 cells were plated at a density of 2×10^4 cells per well onto 24-well transwell inserts with 0.4-µm pore polyethylene terephthalate (PET) membrane (Brand, BR782711), pre-coated with 50 µg/ml rat tail collagen-I. Cells were maintained in DMEM supplemented with 10% FBS and incubated overnight at 37°C in a humidified atmosphere containing 5% CO_2.

ARTICLE IN PRESS

The following day, HPMECs were seeded onto Matrigel in the lower chamber and cultured in EBM as described in the section “Matrigel-based angiogenesis assay and tube quantification”. HPMECs were treated with either 0.1% EtOH (vehicle control) or 10 μM RA.

Prior to co-culture, the medium in the transwell inserts containing A549 cells was removed, and cells were washed three times with PBS to remove any residual serum. Inserts were then replenished with EBM supplemented with 0.2% FCS. After 4 hours of RA or EtOH treatment, transwell inserts containing A549 cells were placed into wells containing HPMECs, initiating co-culture for 2, 4, or 16 hours.

After the 2-hour timepoint, A549 cells in the upper chamber were fixed and subjected to immunostaining for phospho-EGFR and TGFα. Conditioned media from the lower chamber were collected at 4and 16 hours for quantification of extracellular TGFα using the Human TGF-alpha DuoSet ELISA (R&D Systems, DY239), according to the manufacturers’ instructions.

ARTICLE IN PRESS

Statistical analysis

All graphs and statistical tests were produced using GraphPad Prism 10. Data are expressed as mean ± standard error of mean (SEM). The D’Agostino–Pearson test was employed to assess the normality of the data. For non-parametric datasets, the Mann–Whitney *U*-test was utilised for comparisons between two groups, while comparisons involving more than two groups were performed using the Kruskal–Wallis test followed by Dunn’s multiple comparison test. The specific statistical tests applied, sample size (*n*), and the number of experiments conducted are detailed in the figure legends. A *p*-value of less than 0.05 was considered statistically significant.

Data availability

ARTICLE IN PRESS

The microarray data generated or analysed during the current study are available in the Gene Expression Omnibus (GEO) repository under the accession number GSE307491.

Acknowledgements

This study was funded by the Royal Brompton and Harefield Hospitals Charity (Grant 123/P90719) and an award from Mr and Mrs Youssef Mansour. Imaging for this study was conducted in the Facility for Imaging by Light Microscopy (FILM) at Imperial College and was part supported by Wellcome Trust (grant 104931/Z/14/Z). Funders played no role in study design, data collection, analysis, data interpretation of data, or the writing of this manuscript. Graphical abstract (https://BioRender.com/a30g772), Figure 3a (https://BioRender.com/j66c448), and Figure 8a (https://BioRender.com/kcrapgy) were created in BioRender.

Author contributions

CD, MH and S-SC conceived and designed the study. S-SC, CY, RM and DC performed experiments and analysed data. DC and MG provided conceptual advice. S-SC and CD wrote the manuscript. All authors contributed to editing the manuscript. MH and CD acquired funding.

Competing interests: The authors declare no competing financial or non-financial interests.

References

1 Basil, M. C., Alysandratos, K. D., Kotton, D. N. & Morrisey, E. E. Lung repair and regeneration: Advanced models and insights into human disease. *Cell Stem Cell* **31**, 439-454 (2024).

2 Wang, Y., Wang, L., Ma, S., Cheng, L. & Yu, G. Repair and regeneration of the alveolar epithelium in lung injury. *FASEB J* **38**, e23612 (2024).

3 Chen, Y. *et al*. Lung regeneration: diverse cell types and the therapeutic potential. *MedComm (2020)* **5**, e494 (2024). https://doi.org:10.1002/mco2.494

4 Alysandratos, K. D., Herriges, M. J. & Kotton, D. N. Epithelial Stem and Progenitor Cells in Lung Repair and Regeneration. *Annu Rev Physiol* **83**, 529-550 (2021).

ARTICLE IN PRESS

5 Wu, H. & Tang, N. Stem cells in pulmonary alveolar regeneration. *Development* **148** (2021).

6 Crosby, L. M. & Waters, C. M. Epithelial repair mechanisms in the lung. *Am J Physiol Lung Cell Mol Physiol* **298**, L715-731 (2010).

7 McCall, A. S. *et al.* Hypoxia-inducible factor 2 regulates alveolar regeneration after repetitive injury in three-dimensional cellular and in vivo models. *Sci Transl Med* **17**, eadk8623 (2025). https://doi.org:10.1126/scitranslmed.adk8623

8 Juul, N. H., Stockman, C. A. & Desai, T. J. Niche Cells and Signals that Regulate Lung Alveolar Stem Cells In Vivo. *Cold Spring Harb Perspect Biol* **12** (2020). https://doi.org:10.1101/cshperspect.a035717

9 Yang, L. *et al.* FGF/FGFR signaling: From lung development to respiratory diseases. *Cytokine Growth Factor Rev* **62**, 94-104 (2021).

10 Wu, M. *et al.* Shh Signaling from the Injured Lung Microenvironment Drives BMSCs Differentiation into Alveolar Type II Cells for Acute Lung Injury Treatment in Mice. *Stem Cells Int* **2024**, 1823163 (2024).

11 Massaro, G. D. & Massaro, D. Retinoic acid treatment abrogates elastase-induced pulmonary emphysema in rats. *Nat Med* **3**, 675-677 (1997).

12 Hind, M. & Maden, M. Retinoic acid induces alveolar regeneration in the adult mouse lung. *Eur Respir J* **23**, 20-27 (2004).

13 Giordano, R. J. *et al.* Targeted induction of lung endothelial cell apoptosis causes emphysema-like changes in the mouse. *J Biol Chem* **283**, 29447-29460 (2008).

14 Maden, M. & Hind, M. Retinoic acid, a regeneration-inducing molecule. *Dev Dyn* **226**, 237-244 (2003).

15 Ng-Blichfeldt, J. P. *et al.* Deficient retinoid-driven angiogenesis may contribute to failure of adult human lung regeneration in emphysema. *Thorax* **72**, 510-521 (2017).

16 Ding, B. S. *et al.* Endothelial-derived angiocrine signals induce and sustain regenerative lung alveolarization. *Cell* **147**, 539-553 (2011).

17 Hardie, W. D., Piljan-Gentle, A., Dunlavy, M. R., Ikegami, M. & Korfhagen, T. R. Dose-dependent lung remodeling in transgenic mice expressing transforming growth factor-alpha. *Am J Physiol Lung Cell Mol Physiol* **281**, L1088-1094 (2001).

18 Cunningham, T. J. & Duester, G. Mechanisms of retinoic acid signalling and its roles in organ and limb development. *Nat Rev Mol Cell Biol* **16**, 110-123 (2015).

19 Lalevee, S. *et al.* Genome-wide in silico identification of new conserved and functional retinoic acid receptor response elements (direct repeats separated by 5 bp). *J Biol Chem* **286**, 33322-33334 (2011).

20 Coyle, K. M., Maxwell, S., Thomas, M. L. & Marcato, P. Profiling of the transcriptional response to all-trans retinoic acid in breast cancer cells reveals RARE-independent mechanisms of gene expression. *Sci Rep* **7**, 16684 (2017). https://doi.org:10.1038/s41598-017-16687-6

21 Miettinen, P. J. *et al.* Impaired lung branching morphogenesis in the absence of functional EGF receptor. *Dev Biol* **186**, 224-236 (1997). [pii]10.1006/dbio.1997.8593.

22 Burgel, P. R. & Nadel, J. A. Epidermal growth factor receptor-mediated innate immune responses and their roles in airway diseases. *Eur Respir J* **32**, 1068-1081 (2008).

23 Lai, H. & Rogers, D. F. New pharmacotherapy for airway mucus hypersecretion in asthma and COPD: targeting intracellular signaling pathways. *J Aerosol Med Pulm Drug Deliv* **23**, 219-231 (2010).

ARTICLE IN PRESS

ARTICLE IN PRESS

24 Sharma, S. V., Bell, D. W., Settleman, J. & Haber, D. A. Epidermal growth factor receptor mutations in lung cancer. *Nat Rev Cancer* **7**, 169-181 (2007).

25 Puddicombe, S. M. *et al.* Involvement of the epidermal growth factor receptor in epithelial repair in asthma. *FASEB J* **14**, 1362-1374 (2000).

26 Zepp, J. A. & Morrisey, E. E. Cellular crosstalk in the development and regeneration of the respiratory system. *Nat Rev Mol Cell Biol* **20**, 551-566 (2019).

27 Chung, M. I., Bujnis, M., Barkauskas, C. E., Kobayashi, Y. & Hogan, B. L. M. Niche-mediated BMP/SMAD signaling regulates lung alveolar stem cell proliferation and differentiation. *Development* **145** (2018).

28 Ha, H., Debnath, B. & Neamati, N. Role of the CXCL8-CXCR1/2 Axis in Cancer and Inflammatory Diseases. *Theranostics* **7**, 1543-1588 (2017). https://doi.org:10.7150/thno.15625

29 Korfhagen, T. R. *et al.* Respiratory epithelial cell expression of human transforming growth factor-alpha induces lung fibrosis in transgenic mice. *J Clin Invest* **93**, 1691-1699 (1994).

30 Witherden, I. R. & Tetley, T. D. Isolation and Culture of Human Alveolar Type II Pneumocytes. *Methods Mol Med* **56**, 137-146 (2001).

31 Roberts, C. Regulating Retinoic Acid Availability during Development and Regeneration: The Role of the CYP26 Enzymes. *J Dev Biol* **8** (2020).

32 Wang, S., Yu, J., Kane, M. A. & Moise, A. R. Modulation of retinoid signaling: therapeutic opportunities in organ fibrosis and repair. *Pharmacol Ther* **205**, 107415 (2020).

33 Tierney, M. T. *et al.* Vitamin A resolves lineage plasticity to orchestrate stem cell lineage choices. *Science* **383**, eadi7342 (2024).

34 Maden, M. & Hind, M. Retinoic acid, a regeneration-inducing molecule. *Dev Dyn* **226**, 237-244 (2003).

35 Timoneda, J. *et al.* Vitamin A Deficiency and the Lung. *Nutrients* **10** (2018). https://doi.org:10.3390/nu10091132

36 Jones, P. W., Rames, A.D. TESRA: Treatment of Emphysema with a Gamma-selective Retinoid agonist. *Am J Respir Crit Care Med* **183** (2011).

37 Singh, A. B. & Harris, R. C. Autocrine, paracrine and juxtacrine signaling by EGFR ligands. *Cell Signal* **17**, 1183-1193 (2005).

38 Trinh, N. T. *et al.* Involvement of KATP and KvLQT1 K+ channels in EGF-stimulated alveolar epithelial cell repair processes. *Am J Physiol Lung Cell Mol Physiol* **293**, L870-882 (2007).

39 Li, J., Cao, J., Yan, C. & Gong, X. TGF-alpha/EGFR signaling promotes lipopolysaccharide-induced abnormal elastin deposition and alveolar simplification. *Exp Cell Res* **437**, 113997 (2024).

40 Miller, L. A., Zhao, Y. H. & Wu, R. Inhibition of TGF-alpha gene expression by vitamin A in airway epithelium. *J Clin Invest* **97**, 1429-1435 (1996).

41 Lin, S. *et al.* Redundant roles of EGFR ligands in the ERK activation waves during collective cell migration. *Life Sci Alliance* **5** (2022). https://doi.org:10.26508/lsa.202101206

42 Gagliardi, P. A. & Pertz, O. The mitogen-activated protein kinase network, wired to dynamically function at multiple scales. *Curr Opin Cell Biol* **88**, 102368 (2024).

43 Deguchi, E. *et al.* Low-affinity ligands of the epidermal growth factor receptor are long-range signal transmitters in collective cell migration of epithelial cells. *Cell Rep* **43**, 114986 (2024). https://doi.org:10.1016/j.celrep.2024.114986

ARTICLE IN PRESS

44 Luetteke, N. C. *et al.* Targeted inactivation of the EGF and amphiregulin genes reveals distinct roles for EGF receptor ligands in mouse mammary gland development. *Development* **126**, 2739-2750 (1999).

45 Brachmann, R. *et al.* Transmembrane TGF-alpha precursors activate EGF/TGF-alpha receptors. *Cell* **56**, 691-700 (1989).

46 Akram, K. M. *et al.* Time-lapse Imaging of Alveologenesis in Mouse Precision-cut Lung Slices. *Bio Protoc* **9**, e3403 (2019). https://doi.org:10.21769/BioProtoc.3403

47 Cheong, S. S. *et al.* The Planar Polarity Component VANGL2 Is a Key Regulator of Mechanosignaling. *Front Cell Dev Biol* **8**, 577201 (2020). https://doi.org:10.3389/fcell.2020.577201

ARTICLE IN PRESS

ARTICLE IN PRESS

Figure Legends

Figure 1. Increased RA signalling activity following acid injury in mouse PCLS. Histogram showing transcript levels of genes associated with the RA signalling pathway, including RA receptors (*Rara, Rarb*, and *Rarg*), RA synthesis genes (*Aldh1a1, Aldh1a2*, and *Aldh1a3*), and RA degradation genes (*Cyp26a1*, *Cyp26b1*, and *Cyp26c1*), assessed 48 hours after injuring mouse PCLS with 0.1 M HCl. Gene expression was normalised to the housekeeping gene *B2m* and expressed as fold change relative to uninjured control PCLS. n = 4 mice; Mann-Whitney *U*-test, *$p < 0.05$.

Figure 2. RA enhances wound healing and angiogenesis in endothelial cells but does not affect alveolar epithelial A549 cells. (a-b) Representative images showing endothelial tube-like structures. Tube lengths are depicted as green lines, and nodes are indicated by red dots. **(c-d)** Quantification of total tube length **(c)** and number of nodes **(d)** per field of view in HPMECs treated with either EtOH control or 10 μM RA at 90 minutes post-treatment. n = 5 independent experiments; each experiment was run in triplicate; each dot represents the mean value per experiment. Mann-Whitney *U*-test, *$p < 0.05$. **(e)** Representative images of HUVEC wound closure following treatment with 3 μM, 5 μM, and 10 μM RA, compared to EGM positive control and EBM + 0.1% EtOH vehicle controls, at 0 and 19 hours post-scratch. Wound edges are marked with yellow lines. **(f)** Percentage of wound healed measured at 19 hours post-scratch in HUVECs. n = 3 independent experiments; two or three technical replicates per experiment; each dot represents a technical replicate. Data are presented as mean ± SEM; Kruskal-Wallis with Dunn's multiple comparisons test, *$p < 0.05$, ***$p < 0.001$. **(g)** Images of HUVECs treated with 20 μM and 50 μM RA at 0 and 19 hours post-scratch. **(h)** Histogram showing the percentage of wound healing in A549 cells treated with 10 μM RA compared to DMEM + 10% FBS positive control and serum-free DMEM + 0.1% EtOH vehicle controls at 0 and 19 hours post-scratch. n =

ARTICLE IN PRESS

3 independent experiments; each dot represents the mean percentage of wound healed per experiment. Data are presented as mean ± SEM; Kruskal-Wallis with Dunn's multiple comparisons test, *$p < 0.05$.

Figure 3. HPMECs respond to exogenous RA at 4 hours post-treatment. (a) Schematic diagram of the HPMEC angiogenesis assay and the timeline for RNA extraction for microarray profiling using Affymetrix Human U133 Plus 2 GeneChip microarrays. Total RNA was extracted from HPMECs seeded on Matrigel at 0 hours, 40 minutes, and 4 hours after treatment. $n = 4$ independent experiments; each RNA sample was produced by pooling three technical replicates. Diagram was created in BioRender. **(b)** Volcano plot of differentially expressed genes (DEGs) in HPMECs treated with 10 μM RA versus EtOH control at 4 hours. Upregulated genes are shown in red, downregulated genes in green. **(c)** Extrapolated volcano plot highlighting upregulation of key RA signalling components, including *RARB, DHRS3*, *NRIP1*, and *RDH10*, at 4 hours after RA treatment.

ARTICLE IN PRESS

Figure 4. Gene set enrichment analysis and validation of expression change in candidate genes. (a) Histogram showing Gene Ontology (GO) biological process terms enriched in upregulated genes in RA-treated HPMECs, analysed using the Cytoscape STRING enrichment tool. **(b)** Over-represented pathways in RA-treated HPMECs identified by PANTHER and Reactome pathway analyses. Biological processes and pathways are ranked by statistical significance. **(c-e)** Transcript levels of *BMP2* **(c)**, *CXCL8* **(d)**, and *TGFA* **(e)** in EtOH control or 10 μM RA-treated HPMEC monolayers or HPMECs undergoing angiogenesis. $n = 4$ independent experiments; each experiment was run in triplicate. Data are presented as mean ± SEM; Mann–Whitney *U*-test, *$p < 0.05$.

ARTICLE IN PRESS

Figure 5. TGFα promotes wound healing and cell migration in A549 and primary human AT2 cells. (a) Representative images showing A549 cells treated with DMEM + 10% FBS (positive control), DMEM + 0.5% FBS (negative control), or 40 ng/ml TGFα at 0 and 24 hours post-scratch. Wound edges are marked with green lines. **(b)** Histogram of wound closure at 24 hours post-scratch in A549 cells treated with controls or increasing concentrations of TGFα (0.1 ng/ml, 0.2 ng/ml, 0.4 ng/ml, 4 ng/ml, and 40 ng/ml). **(c)** Percentage of Ki67-positive cells in A549 treated with varying TGFα concentrations, normalised to total DAPI-positive nuclei. $n = 3$ independent experiments; each experiment was run in duplicate or triplicate. Data are presented as mean ± SEM; Kruskal-Wallis with Dunn's multiple comparisons test, $*p < 0.05$, $***p < 0.001$. **(d)** Representative images of hAT2 cells treated with hybridoma medium + 1% FBS (negative control) or 4 ng/ml TGFα at 0 and 24 hours post-migration. Green lines indicate cell-free areas. **(e)** Quantification of hAT2 migration at 24 hours after treatment with hybridoma medium + 10% FBS (positive control), hybridoma medium + 1% FBS (negative control), or increasing TGFα concentrations (0.2 ng/ml, 0.4 ng/ml, 1 ng/ml, and 4 ng/ml). **(f)** Quantification of Ki67-positive hAT2 cells treated with different TGFα concentrations. *n* = hAT2 cells isolated from 3 donors; two or three technical replicates per experiment; each dot represents a technical replicate. Data are presented as mean ± SEM; Kruskal-Wallis with Dunn's multiple comparisons test, $*p < 0.05$, $***p < 0.001$. **(g)** Images showing hAT2 cells labelled with NucView® 488 Caspase-3 dye (green) to detect apoptotic cells at the experiment endpoint. Nuclei were counterstained with DAPI (blue). Hybridoma medium + 1% FBS served as negative control; 70% methanol as positive control for apoptosis. Images were captured using an inverted Zeiss Axio Observer widefield epifluorescence microscope.

ARTICLE IN PRESS

Figure 6. TGFα does not affect cell migration in HLFs or HPMECs. (a) Representative images of HLFs treated with DMEM + 1% FBS (negative control) or 4 ng/ml TGFα at 0 and 16 hours post-scratch. White lines indicate wound areas. **(b)** Histogram illustrating cell migration rates at 16 hours in HLFs incubated with DMEM + 10% FBS (positive control), DMEM + 1% FBS (negative control), and varying concentrations of recombinant TGFα (0.2 ng/ml, 0.4 ng/ml, and 4 ng/ml). **(c)** Percentage of Ki67-positive HLFs after treatment with different concentrations of TGFα. *n* = HLFs isolated from 3 donors; two or three technical replicates per experiment; each dot represents a technical replicate. Data are presented as mean ± SEM; Kruskal-Wallis with Dunn's multiple comparisons test, $*p < 0.05$. **(d)** Representative images of HLFs stained with NucView® 488 Caspase-3 dye (green) and DAPI (cyan). DMEM + 1% FBS served as negative control; 70% methanol as positive control. Images were captured on a Leica SP8 inverted confocal microscope with a HC PL APO 40×/1.30 oil objective lens. **(e-f)** Wound closure at 0 and 16 hours **(e),** and quantification of wound healing **(f)** in HPMECs treated with EBM + 5% FCS (positive control), EBM + 2% FCS (negative control), 4 ng/ml, or 40 ng/ml TGFα. Green lines indicate wound edges. *n* = 1 experiment; two or three technical replicates per experiment; each dot represents a technical replicate. Data are presented as mean ± SEM.

Figure 7. EGFR activation in A549 cells treated with exogenous TGFα or EGF. (a-c) Representative immunofluorescence images of untreated A549 cells (serum-free medium, negative control) or treated with 40 ng/ml TGFα or 50 ng/ml EGF for 30 minutes **(a)** or 2 hours **(b-c)**. Cells were immunostained for phospho-EGFR Y1068 (magenta), and nuclei were counterstained with DAPI (cyan). Images were captured using a Leica SP8 inverted confocal microscope with a HC PL APO 40×/1.30 oil objective lens. *n* = 2 independent experiments; three technical replicates per experiment.

ARTICLE IN PRESS

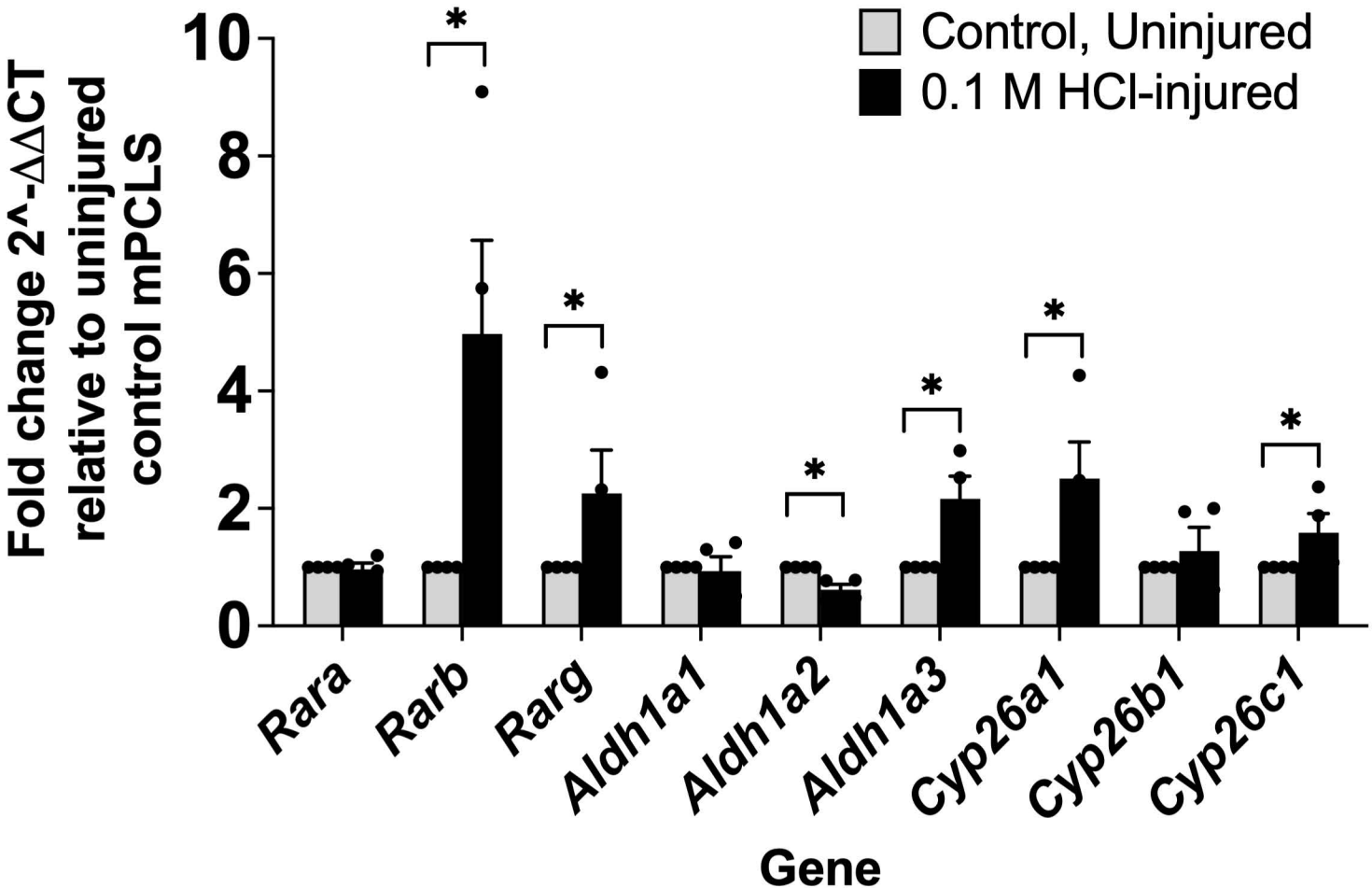
Figure 8. Membrane-associated TGFα and EGFR activation in A549 cells co-cultured with RA-treated HPMECs. (a) Schematic of the HPMEC–A549 transwell co-culture system. A549 cells were cultured in the upper chamber and co-cultured with HPMECs seeded on Matrigel in the lower chamber with either 0.1% EtOH or 10 μM RA. Diagram was created in BioRender. **(b-c)** Representative immunofluorescence images of A549 cells following 2 hours of co-culture with EtOH control-treated HPMECs **(b)**, RA-treated HPMECs **(c).** Higher magnification images are shown on the right panel. **(c)** Arrows indicate the distribution of TGFα and phospho-EGFR at the cell membrane in A549 cells co-cultured with RA-treated HPMECs. **(d)** Control experiment showing A549 cells treated with RA in the absence of HPMECs. A549 cells were immunostained for phospho-EGFR (yellow) and TGFα (magenta). Nuclei were counterstained with DAPI (cyan). Images were captured on a Leica SP8 inverted confocal microscope with a HC PL APO 40×/1.30 oil objective lens. *n* = 2 independent experiments; three technical replicates per experiment.

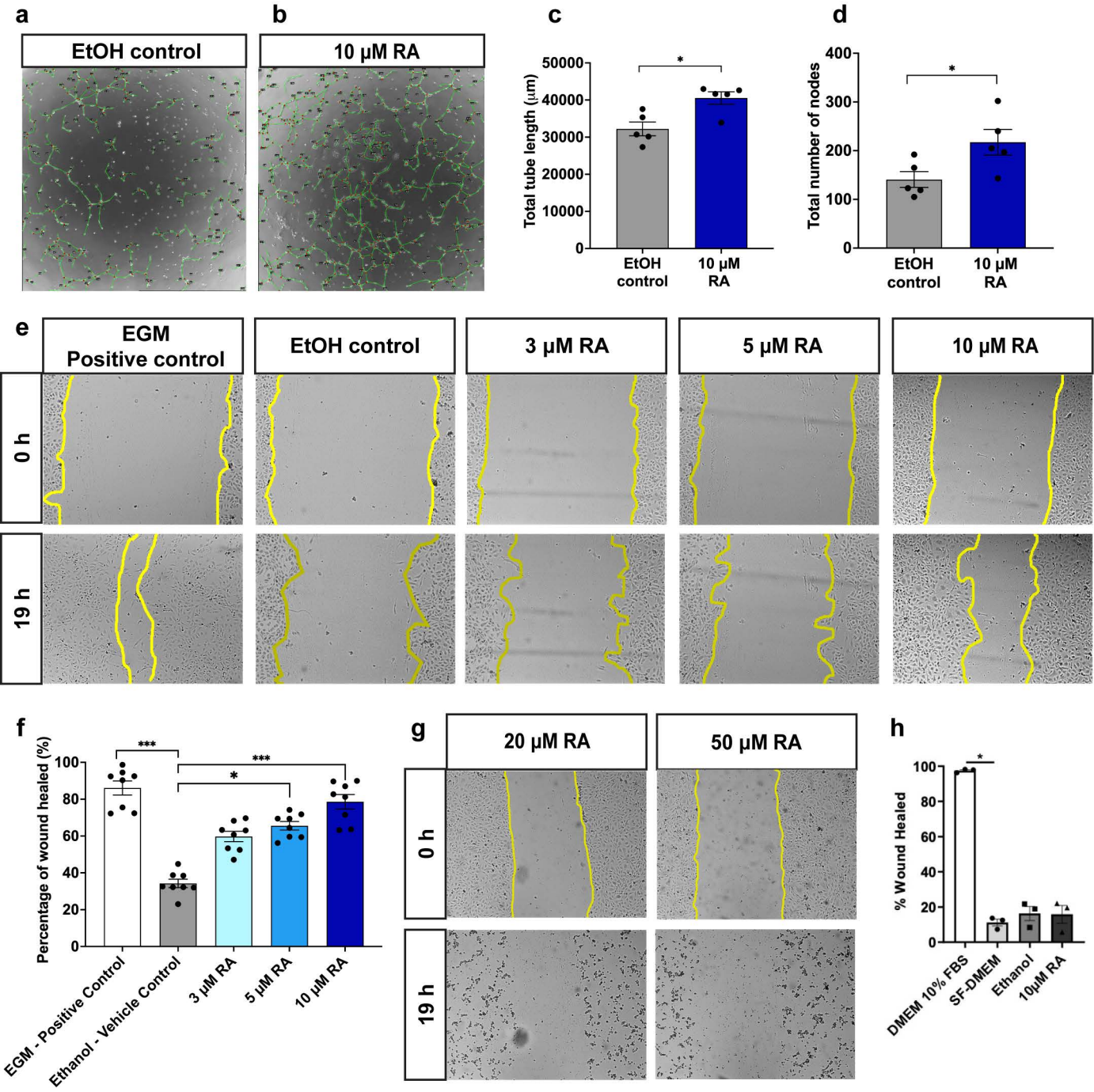
Gene symbol	Protein class	Mapped to signalling pathway	Fold Change	FDR *P*-value
CXCL8	chemokine	CCKR signalling map, Interleukin signalling pathway, Inflammation mediated by chemokine and cytokine signalling pathway	9.24	2.56E-07
TGFA	growth factor	EGF receptor signalling pathway	4.56	0.0176
BMP2	growth factor	TGF-beta signalling pathway, Gonadotropin-releasing hormone receptor pathway	3.57	0.0004
FGF20	growth factor	FGF signalling pathway	2.88	0.0184

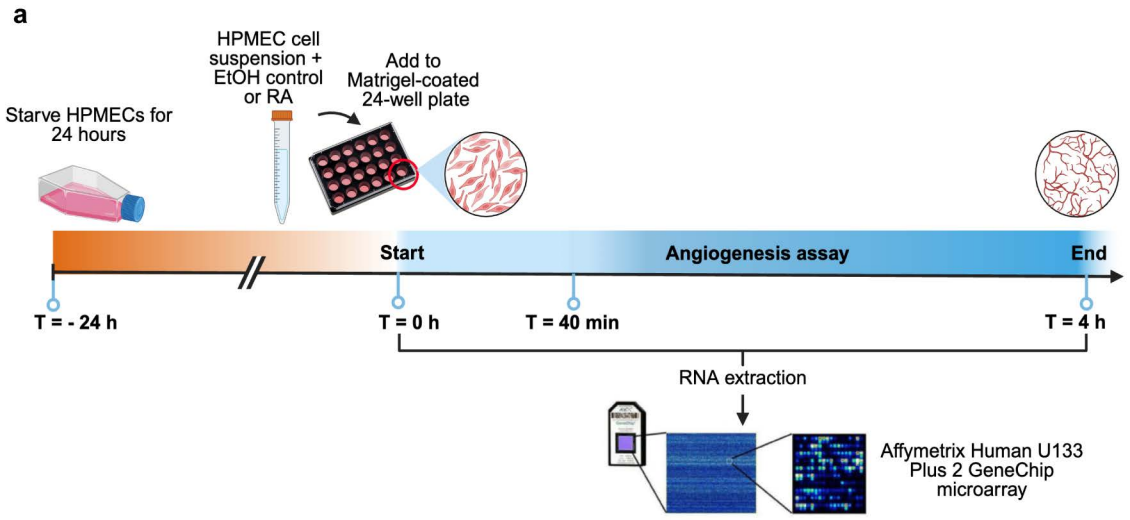
ARTICLE IN PRESS

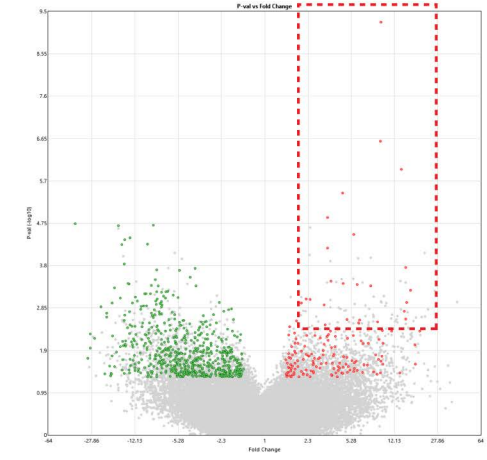
WNT9A	intercellular signal molecule	Wnt signalling pathway, cadherin signalling pathway	2.02	0.0376
GDF15	growth factor	TGF-beta signalling pathway	1.79	0.0087
EFNB1	membrane-bound signalling molecule	Angiogenesis	1.7	0.0286
ADM	peptide hormone	-	1.58	0.0303
CCL23	cytokine	-	-9.12	0.0188
WNT5A	intercellular signal molecule	Angiogenesis, Wnt signalling pathway, cadherin signalling pathway	-8.18	0.0167
PDYN	neuropeptide	Enkephalin release, Opioid prodynorphin pathway, Opioid proenkephalin pathway	-4.05	0.0241
PTN	growth factor		-3.34	0.0473
FGF5	growth factor	FGF signalling pathway	-2.22	0.0129
FGF8	growth factor	FGF signalling pathway	-2.11	0.0484

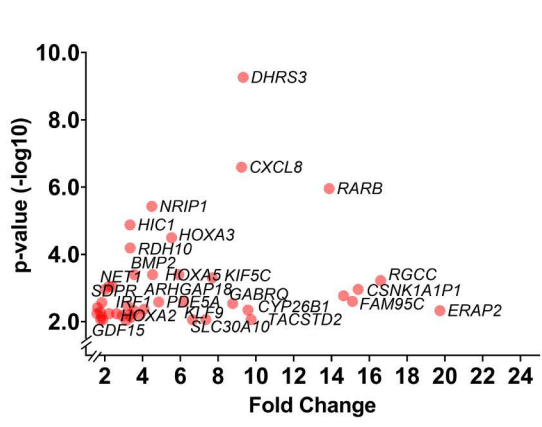
Table 1. Identification of 14 genes encoding intercellular signalling proteins.

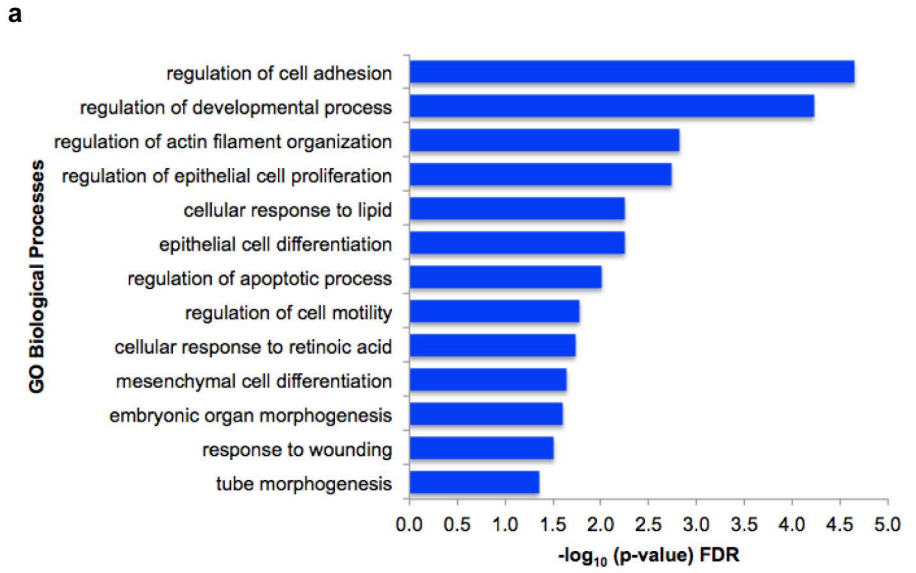

Control, Uninjured
0.1 M HCl-injured
Fold change 2^-ΔΔCT relative to uninjured control mPCLS
10
8
6
4
2
0
*
Rara
Rarb
Rarg
Aldh1a1
Aldh1a2
Aldh1a3
Cyp26a1
Cyp26b1
Cyp26c1
Gene

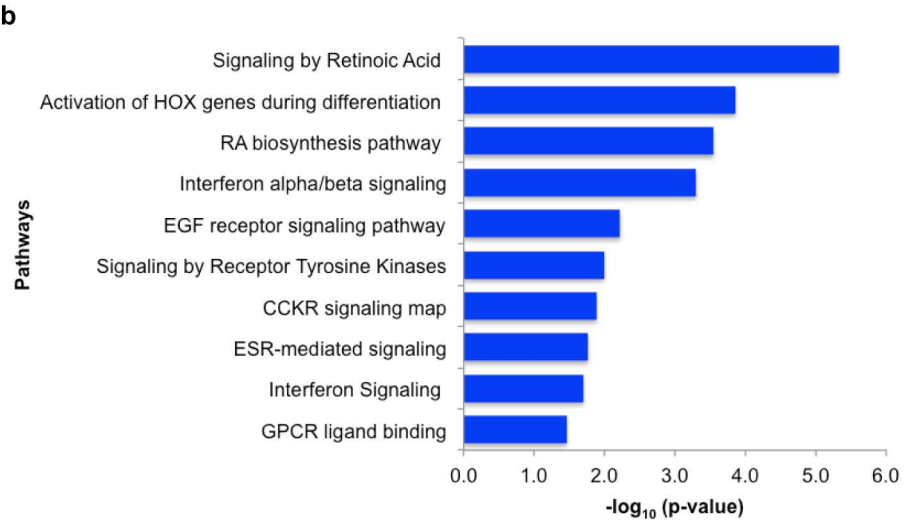

a
EtOH control
b
10 μM RA
c
Total tube length (μm)
50000
40000
30000
20000
10000
0
*
EtOH control
10 μM RA
d
Total number of nodes
400
300
200
100
0
*
EtOH control
10 μM RA
e
EGM Positive control
EtOH control
3 μM RA
5 μM RA
10 μM RA
0 h
19 h
f
Percentage of wound healed (%)
100
80
60
40
20
0
***
***
*
EGM - Positive Control
Ethanol - Vehicle Control
3 μM RA
5 μM RA
10 μM RA
g
20 μM RA
50 μM RA
0 h
19 h
h
% Wound Healed
100
80
60
40
20
0
*
DMEM 10% FBS
SF-DMEM
Ethanol
10μM RA

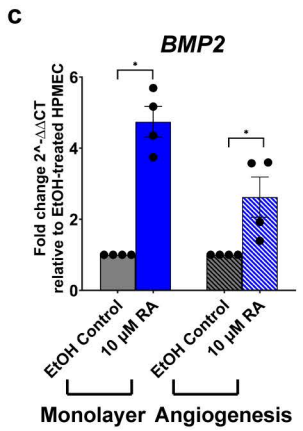

a
HPMEC cell suspension + EtOH control or RA
Add to Matrigel-coated 24-well plate
Starve HPMECs for 24 hours
Start
Angiogenesis assay
End
T = - 24 h
T = 0 h
T = 40 min
T = 4 h
RNA extraction
Affymetrix Human U133 Plus 2 GeneChip microarray

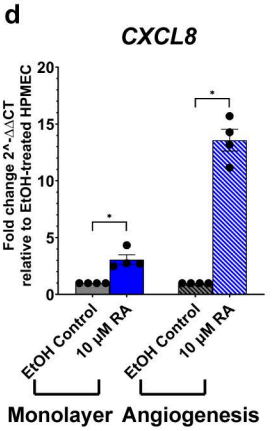

b
P-val vs Fold Change
Fold Change

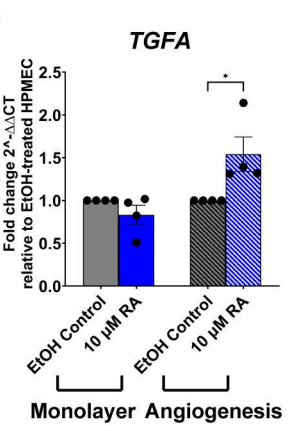

c
p-value (-log10)
Fold Change
DHRS3
CXCL8
RARB
NRIP1
HIC1
HOXA3
RDH10
BMP2
NET1
HOXA5
KIF5C
SDPR
ARHGAP18
GABRQ
IRF1
PDE5A
CYP26B1
HOXA2
KLF9
TACSTD2
GDF15
SLC30A10
RGCC
CSNK1A1P1
FAM95C
ERAP2

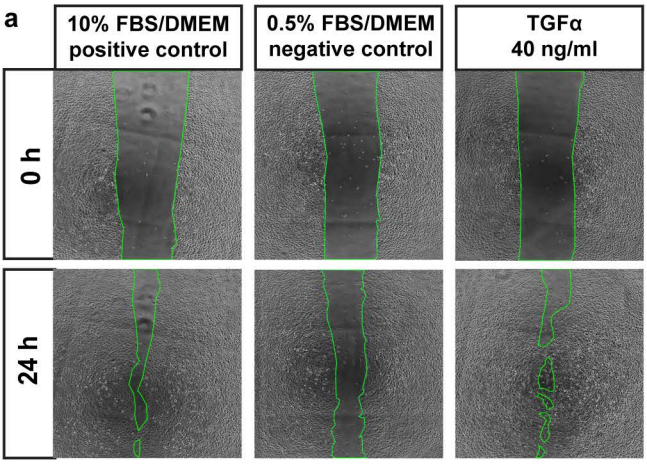

a
GO Biological Processes
regulation of cell adhesion
regulation of developmental process
regulation of actin filament organization
regulation of epithelial cell proliferation
cellular response to lipid
epithelial cell differentiation
regulation of apoptotic process
regulation of cell motility
cellular response to retinoic acid
mesenchymal cell differentiation
embryonic organ morphogenesis
response to wounding
tube morphogenesis
0.0 0.5 1.0 1.5 2.0 2.5 3.0 3.5 4.0 4.5 5.0
-log10 (p-value) FDR

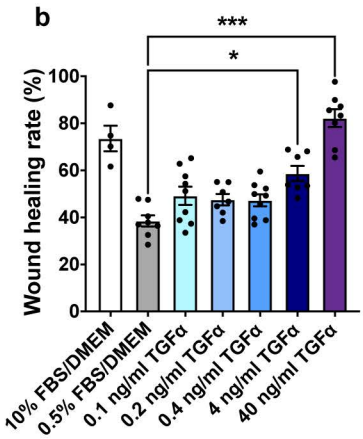

b
Pathways
Signaling by Retinoic Acid
Activation of HOX genes during differentiation
RA biosynthesis pathway
Interferon alpha/beta signaling
EGF receptor signaling pathway
Signaling by Receptor Tyrosine Kinases
CCKR signaling map
ESR-mediated signaling
Interferon Signaling
GPCR ligand binding
0.0 1.0 2.0 3.0 4.0 5.0 6.0
-log10 (p-value)

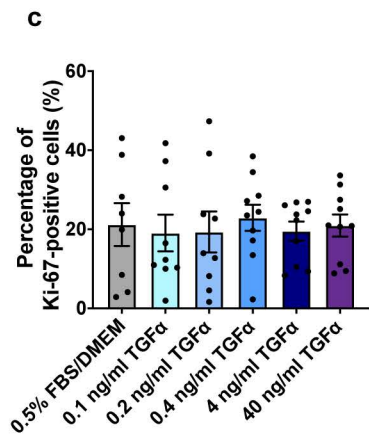

c
BMP2
Fold change 2^-ΔΔCT relative to EtOH-treated HPMEC
EtOH Control
10 μM RA
EtOH Control
10 μM RA
Monolayer
Angiogenesis

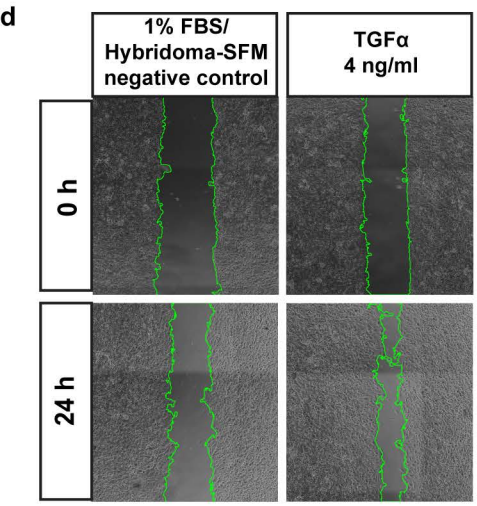

d
CXCL8
Fold change 2^-ΔΔCT relative to EtOH-treated HPMEC
EtOH Control
10 μM RA
EtOH Control
10 μM RA
Monolayer
Angiogenesis

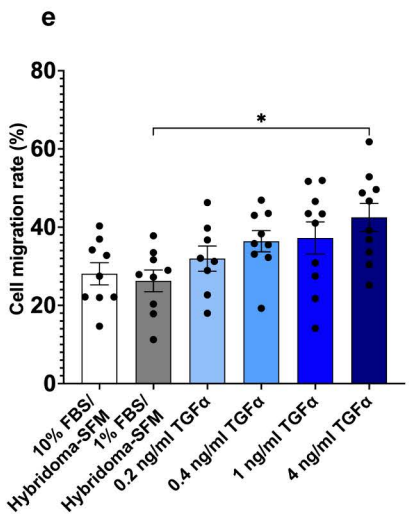

e
TGFA
Fold change 2^-ΔΔCT relative to EtOH-treated HPMEC
EtOH Control
10 μM RA
EtOH Control
10 μM RA
Monolayer
Angiogenesis

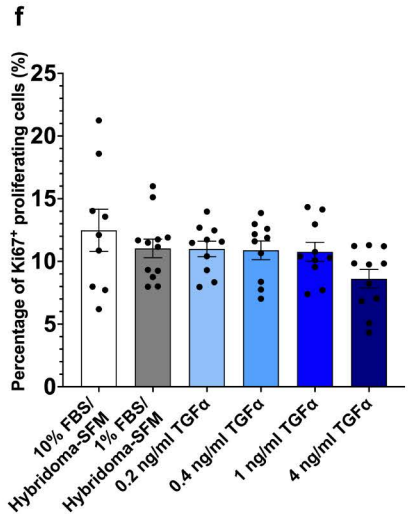

a
10% FBS/DMEM
positive control
0.5% FBS/DMEM
negative control
TGFα
40 ng/ml
0 h
24 h

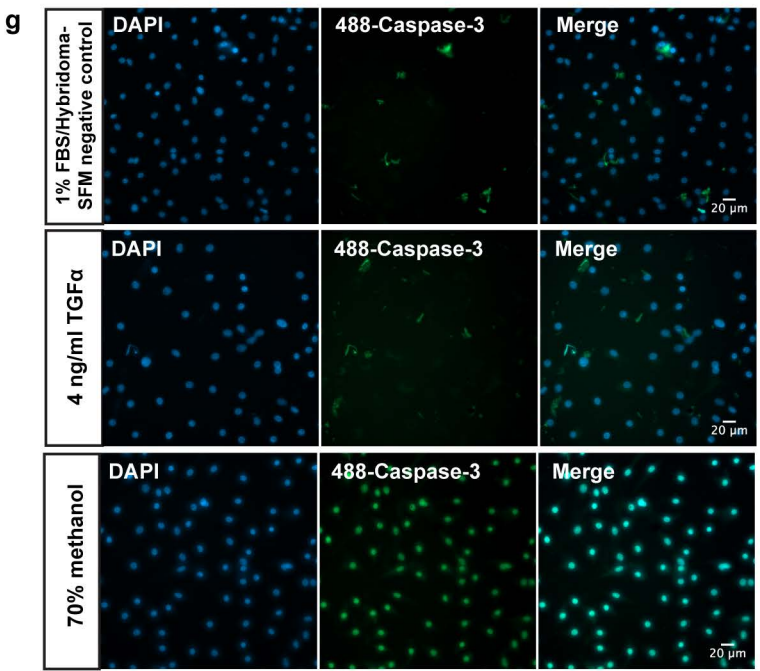

b
***
*
Wound healing rate (%)
100
80
60
40
20
0
10% FBS/DMEM
0.5% FBS/DMEM
0.1 ng/ml TGFα
0.2 ng/ml TGFα
0.4 ng/ml TGFα
4 ng/ml TGFα
40 ng/ml TGFα

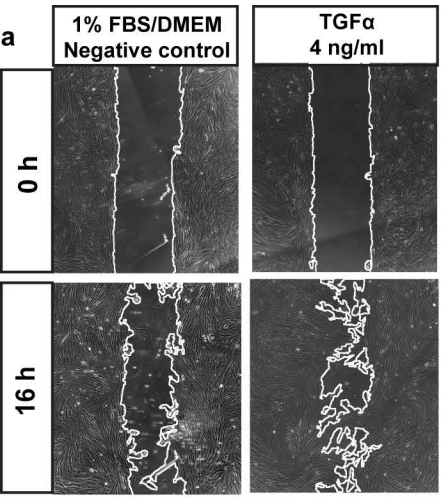

c
Percentage of
Ki-67-positive cells (%)
60
40
20
0
0.5% FBS/DMEM
0.1 ng/ml TGFα
0.2 ng/ml TGFα
0.4 ng/ml TGFα
4 ng/ml TGFα
40 ng/ml TGFα

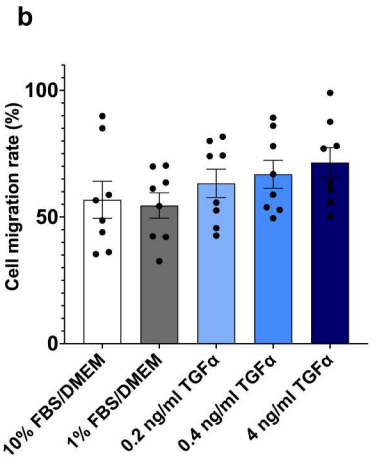

d
1% FBS/
Hybridoma-SFM
negative control
TGFα
4 ng/ml
0 h
24 h

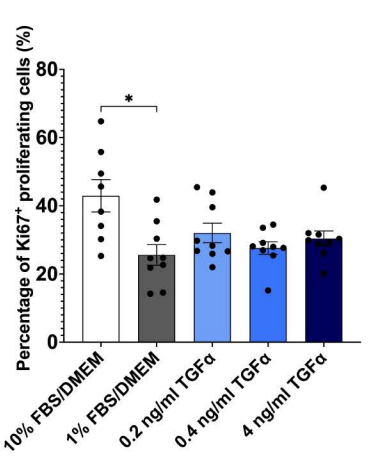

e
*
Cell migration rate (%)
80
60
40
20
0
10% FBS/
Hybridoma-SFM
1% FBS/
Hybridoma-SFM
0.2 ng/ml TGFα
0.4 ng/ml TGFα
1 ng/ml TGFα
4 ng/ml TGFα

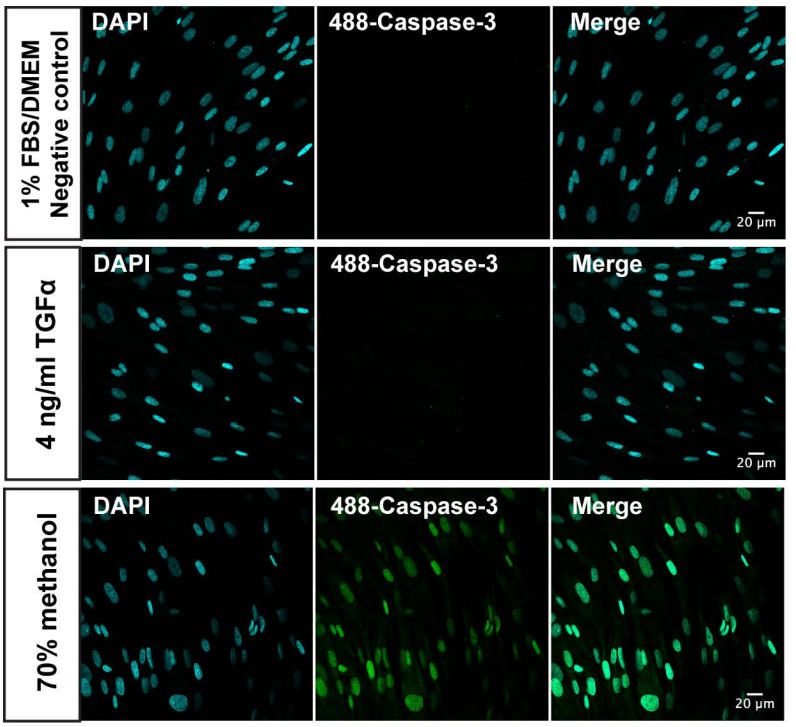

f
Percentage of Ki67+ proliferating cells (%)
25
20
15
10
5
0
10% FBS/
Hybridoma-SFM
1% FBS/
Hybridoma-SFM
0.2 ng/ml TGFα
0.4 ng/ml TGFα
1 ng/ml TGFα
4 ng/ml TGFα

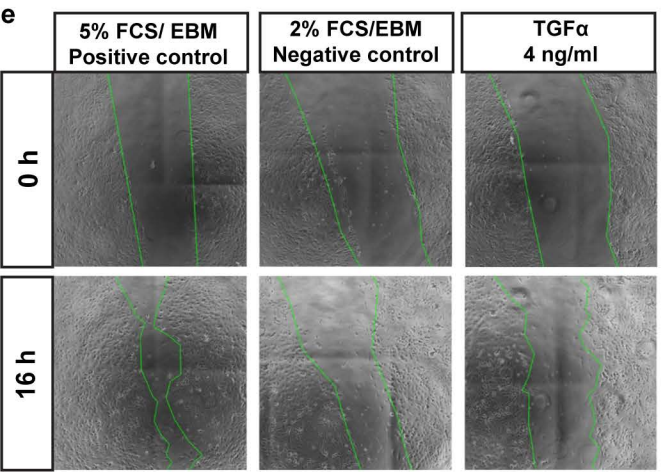

g
1% FBS/Hybridoma-
SFM negative control
4 ng/ml TGFα
70% methanol
DAPI
488-Caspase-3
Merge
20 μm

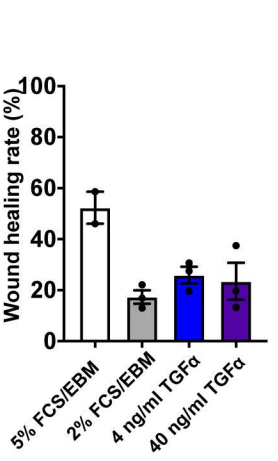

a
1% FBS/DMEM
Negative control
TGFα
4 ng/ml
0 h
16 h

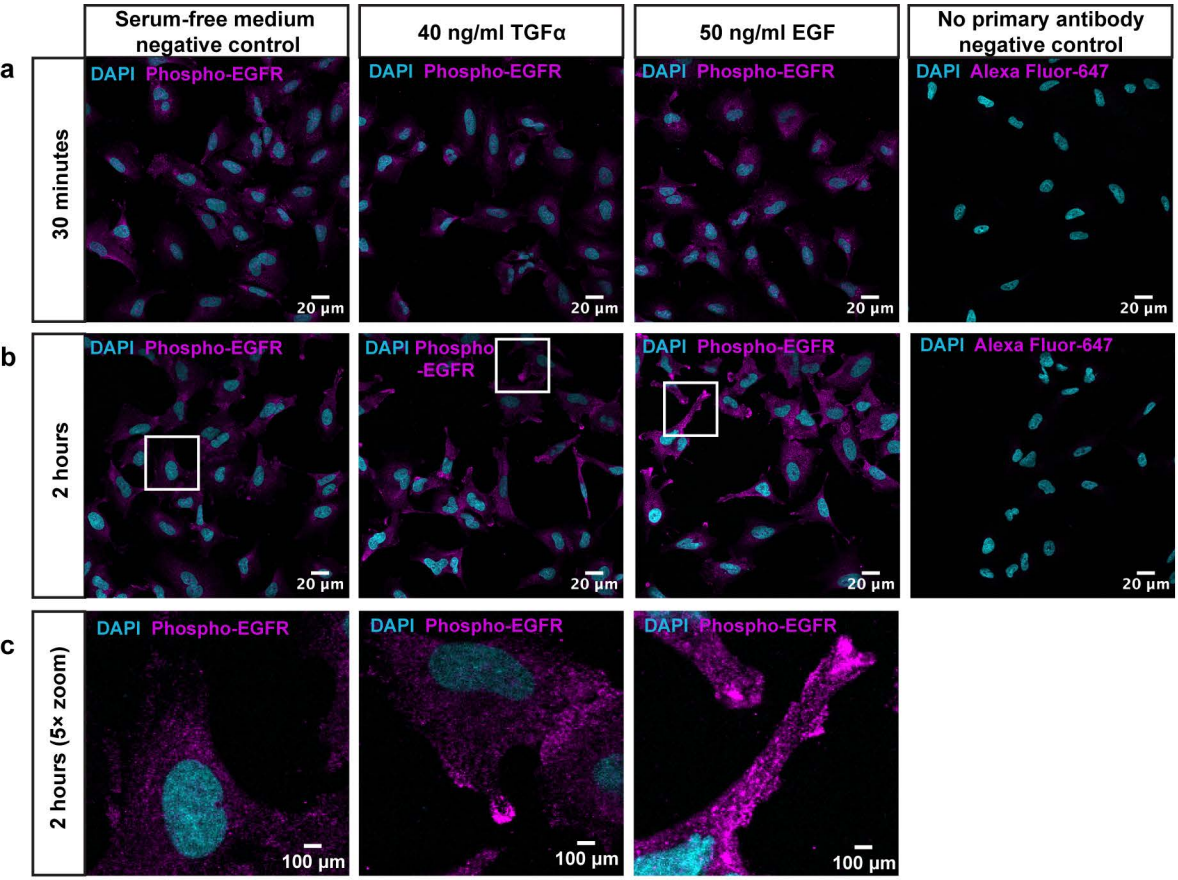

b
Cell migration rate (%)
100
50
0
10% FBS/DMEM
1% FBS/DMEM
0.2 ng/ml TGFα
0.4 ng/ml TGFα
4 ng/ml TGFα

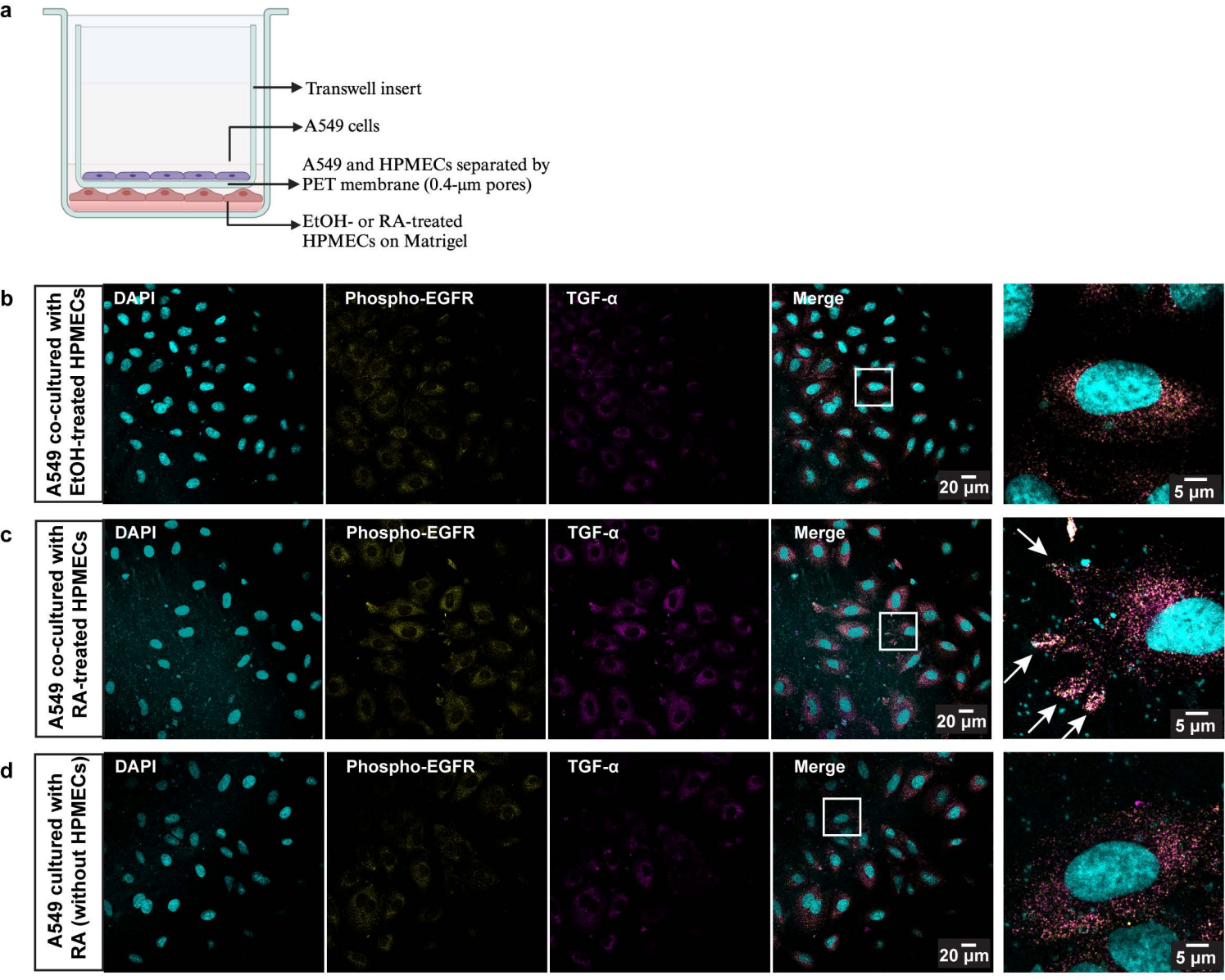

c
Percentage of Ki67+ proliferating cells (%)
80
60
40
20
0
*
10% FBS/DMEM
1% FBS/DMEM
0.2 ng/ml TGFα
0.4 ng/ml TGFα
4 ng/ml TGFα


d
1% FBS/DMEM
Negative control
4 ng/ml TGFα
70% methanol
DAPI
488-Caspase-3
Merge
20 µm


e
5% FCS/ EBM
Positive control
2% FCS/EBM
Negative control
TGFα
4 ng/ml
0 h
16 h


f
Wound healing rate (%)
100
80
60
40
20
0
5% FCS/EBM
2% FCS/EBM
4 ng/ml TGFα
40 ng/ml TGFα


Serum-free medium negative control
40 ng/ml TGFα
50 ng/ml EGF
No primary antibody negative control
a
30 minutes
b
2 hours
c
2 hours (5× zoom)
DAPI Phospho-EGFR
DAPI Alexa Fluor-647
20 µm
100 µm


a
Transwell insert
A549 cells
A549 and HPMECs separated by
PET membrane (0.4-μm pores)
EtOH- or RA-treated
HPMECs on Matrigel
b
A549 co-cultured with
EtOH-treated HPMECs
DAPI
Phospho-EGFR
TGF-α
Merge
20 μm
5 μm
c
A549 co-cultured with
RA-treated HPMECs
DAPI
Phospho-EGFR
TGF-α
Merge
20 μm
5 μm
d
A549 cultured with
RA (without HPMECs)
DAPI
Phospho-EGFR
TGF-α
Merge
20 μm
5 μm